Accepted for publication in *Journal of Geophysical Research*.

SBUV Observations of PMCs Over Two Solar Cycles

Matthew T. DeLand[1], *Eric P. Shettle*[2], *Gary E. Thomas*[3], *John J. Olivero*[4]
[1]Science Systems and Applications, Inc., Lanham, MD
[2]Naval Research Laboratory, Code 7227, Washington, DC
[3]LASP, University of Colorado, Boulder, CO
[4]Embry-Riddle University, Dept. of Physical Sciences, Daytona Beach, FL

Abstract. Previous satellite measurements have provided nearly complete seasonal and geographic coverage of polar mesospheric clouds (PMC), but previous data sets have not been able to evaluate changes in PMC behavior on decadal time scales. The SBUV series of ozone measuring instruments have been flying continuously since 1978. While the instrument design is not optimized for PMC detection, the radiance data can be analyzed to examine the occurrence frequency and intensity of relatively bright PMCs. In this paper, we present PMC results from five SBUV and SBUV/2 instruments covering 23+ years (1978-2002), starting just before the maximum of solar cycle 21 and extending through the maximum of solar cycle 23. The overlapping data sets from nearly identical instruments give an accurate picture of long-term variations. Multiple linear regression fits are used to examine solar and secular correlations. PMC occurrence frequency is anti-correlated with solar Lyman alpha irradiance, with an approximate 0.5-year phase lag in the Northern Hemisphere (R_{solar} = –0.87) and no phase lag in the Southern Hemisphere (R_{solar} = –0.65). The distribution of cloud brightness by season appears to be changing over time. When the PMC brightness for each season is characterized using an exponential cumulative distribution function, the exponent decreases in magnitude by a factor of 2 from 1978 to 2002 in the Southern Hemisphere (R_{time} = +0.85). This implies an increase in the relative proportion of the brightest PMCs. The secular brightness trend is less significant in the Northern Hemisphere (R_{time} = +0.58). We discuss possible origins for these changes.

1. Introduction

The summer night sky at high latitudes is sometimes decorated with ethereal light scattered from layers of particles high above the Earth's surface. Such observations were first documented by Northern Hemisphere observers in the 1880s, and have continued for more than a century. This phenomenon was given the name "noctilucent cloud" (often abbreviated as NLC) to signify their remarkable brightness when observed shortly after sunset. Later measurements showed that NLC occurred at altitudes of 80-85 km, well above any normal cloud. These "clouds at the edge of space" continue to delight us, as well as challenging our understanding of our atmospheric environment.

The Orbiting Geophysical Observatory (OGO-6) satellite provided the first measurements of these scattering layers from space [*Donahue et al.*, 1972]. The first extended set of satellite observations came from the UltraViolet Spectrometer (UVS) on the Solar Mesosphere Explorer satellite (SME), as discussed by *Olivero and Thomas* [1986] and *Thomas and Olivero*

[1989]. These studies suggested the name "polar mesospheric clouds" (PMC) to characterize these space-based observations [*Thomas*, 1984]. Additional PMC observations have been reported for measurements made by the Solar Backscatter Ultraviolet (SBUV) instrument on Nimbus-7 [*Thomas et al.*, 1991], the Wind Imaging Interferometer (WINDII) on UARS [*Evans et al.*, 1995], the Polar Ozone and Aerosol Measurement (POAM II) instrument on SPOT-3 [*Debrestian et al.*, 1997], the Ultraviolet and Visible Imaging and Spectrographic Imaging (UVISI) experiment on MSX [*Carbary et al.*, 1999], the Stratospheric and Aerosol Gas Experiment (SAGE II) [*Burton and Thomason*, 2000], and the Student Nitric Oxide Experiment (SNOE) [*Bailey et al.*, 2001]. In all cases, the satellite measurements are made during local daylight, and thus are not coincident in time with NLC observations. Nevertheless, the conditions deduced for both PMC and NLC formation are essentially identical. We will generally use the term PMC in this paper, with the understanding that NLC are included.

The simplest description of a polar mesospheric cloud is a scattering layer located near the mesopause (80-85 km). High latitude summer mesopause temperatures are the lowest found on Earth, typically reaching 130 K [*Lübken*, 1999]. Such low temperatures imply that the particles comprising PMCs are some form of condensate. *Hervig et al.* [2001] recently provided strong evidence that PMC consist of water ice. *Stevens et al.* [2001] have shown from MAHRSI and CRISTA satellite measurements that supersaturation is not always required for PMC existence, nor is it sufficient. Thus, we anticipate that PMC observations will be dependent on water vapor concentration and mesospheric temperature. Both of these quantities are expected to be sensitive to solar activity variations and long-term climate change. *Thomas et al*. [1991] used observations from the Nimbus-7 SBUV instrument to demonstrate a solar activity dependence in PMC frequency. *Shettle et al.* [2002a] used three satellite data sets to show that "decadal change" occurred between the 1980s and the 1990s. In both cases, however, individual data sets cover only a portion of a solar cycle. Data from the SAGE II instrument have recently been analyzed to produce a 16-year data set covering 1.5 solar cycles [*Shettle et al.*, 2002b].

Another approach is to use multiple, similar satellite instruments that overlap in time, and ideally span more than a single solar cycle. Such data are available from the SBUV series of instruments (SBUV, SBUV/2) flying on Nimbus-7, NOAA-9, NOAA-11, NOAA-14, and NOAA-16 satellites from 1978 through the present. The primary purpose of the SBUV instruments is to monitor the global distribution of the stratospheric vertical profile and total column abundance of ozone. The instrument design, orbit, and data processing algorithm have been maintained with minimal changes to provide long-term continuity of the ozone record. *Thomas et al.* [1991] demonstrated that the radiance data from Nimbus-7 SBUV could also be used to derive the presence and intensity of PMCs. This paper presents PMC results from five separate SBUV-series instruments spanning more than 23 years. Section 2 discusses the SBUV and SBUV/2 instruments and their in-flight performance. Section 3 describes the SBUV PMC detection algorithm used in this study, which is derived from the procedure used by *Thomas et al.* [1991]. Section 4 presents SBUV PMC results for both Northern Hemisphere and Southern Hemisphere seasons from 1978 through 2002. Statistical techniques are also introduced to allow quantitative comparisons between data from different instruments. Section 5 discusses the SBUV PMC results in the context of solar activity variations and long-term climate change. Finally, Section 6 provides concluding remarks.

2. SBUV-type Instruments

The backscattered ultraviolet (buv) technique for the measurement of stratospheric ozone was first proposed by *Twomey* [1961], and elaborated by *Mateer et al.* [1971]. The basic method uses measurements of Earth radiance at discrete wavelengths in the mid-ultraviolet, coupled with periodic measurements of solar irradiance at the same wavelengths. Albedo values are calculated for each wavelength, then inverted using a radiative transfer algorithm to retrieve the ozone profile [*Klenk et al.*, 1980]. The first operational satellite instrument to use this technique was the Nimbus-4 Backscattered Ultraviolet (BUV) instrument, launched in April 1970 [*Heath et al.*, 1973; *Krueger et al.*, 1973]. Nimbus-4 BUV operated until August 1977, but power constraints severely limited data coverage after July 1972 [*Stolarski et al.*, 1997]. Nimbus-4 BUV data were significantly affected by proximity to the South Atlantic Anomaly (SAA) [*McPeters*, 1980]. Since we have not yet evaluated quantitative corrections for this effect, PMC analysis of BUV data will not be presented in this paper. The Nimbus-7 Solar Backscatter Ultraviolet (SBUV) instrument was modified to add a chopper wheel to eliminate SAA effects in radiance measurements [*Heath et al.*, 1975]. SBUV also stowed the solar diffuser when not in use, in order to reduce degradation. This instrument was launched in October 1978 into a 950 km sun-synchronous orbit with a period of 104 minutes. Data quality began to deteriorate after February 1987, when the chopper wheel began to lose synchronization, but measurements continued until June 1990 [*Gleason and McPeters*, 1995]. Both Nimbus-4 and Nimbus-7 flew in Sun-synchronous orbits with Equator-crossing times near 1200 UT, and made ascending node observations up to ~81° latitude. During summer months, descending node measurements were also made at high solar zenith angles (SZA ≈ 72-88°), at latitudes back down to ~ 68°.

A second-generation SBUV instrument (SBUV/2) was developed for NOAA to be flown on Polar Orbiting Environmental System (POES) operational satellites. The NOAA POES series of satellites fly in sun-synchronous polar orbits at an altitude of approximately 850 km and a 98.9° inclination angle. The SBUV/2 instrument has two modifications that affect the PMC measurements. It has a programmable grating drive to permit changes in wavelength selection after launch, and an on-board calibration system to monitor changes in the reflectivity of the solar diffuser and develop a more accurate long-term instrument characterization. The first SBUV/2 instrument was flown on the NOAA-9 satellite, launched in December 1984 [*Frederick et al.*, 1986]. Additional SBUV/2 instruments have been flown on the NOAA-11, NOAA-14, and NOAA-16 satellites. Table 1 lists the periods of data available from these instruments. Note that Nimbus-7 SBUV, NOAA-9 SBUV/2, and NOAA-11 SBUV/2 all collected ozone profile data for more than 12 years, and that NOAA-14 SBUV/2 has operated for more than 7 years so far. The most recent SBUV/2 instrument was launched on NOAA-17 in June 2002, and two additional instruments are scheduled for launch in 2004 and 2008. The long lifetimes of the SBUV and SBUV/2 instruments, and overlap between multiple instruments, provides the basis for a continuous multi-decade PMC data set. In further instrument and algorithm discussions, we use the term “SBUV/2” to refer to any of the BUV, SBUV, or SBUV/2 instruments unless specifically stated otherwise.

The SBUV/2 instrument is an Ebert-Fastie double monochromator that views the Earth with a nadir-pointing 11.3°x11.3° field of view, corresponding to a footprint of ~170x170 km at the surface. During standard operations, 12 wavelengths between 252-340 nm are sampled se-

quentially during each 32-second scan. The nominal wavelength set for SBUV/2 is listed in Table 2. Additional instrument operation details are available in *DeLand et al.* [2001]. All measurements are corrected for time-dependent and wavelength-dependent changes in instrument gain, non-linearity, PMT temperature dependence, and instrument response. Further discussion of long-term calibration corrections is given in *Ahmad et al.* [1994] and *Hilsenrath et al.* [1995]. SBUV/2 measurements are processed by NOAA/NESDIS using the NASA V6 algorithm [*Bhartia et al.*, 1996], and output to Product Master File (PMF) data sets. The radiance values are stored as Q-values, defined as follows [*McPeters*, 1980]:

$$Q_\lambda = \frac{I_\lambda}{F_\lambda \beta_\lambda P(\theta)} \qquad [2.1]$$

where I_λ is the backscattered radiance for wavelengths less than 297.5 nm, F_λ is the extraterrestrial solar irradiance divided by 4π, β_λ is the Rayleigh scattering coefficient, and $P(\theta)$ is the Rayleigh scattering phase function. We remove the Rayleigh scattering and phase function terms to recover the albedo value, A_λ, at each wavelength for further analysis.

$$A_\lambda = \beta_\lambda P(\theta) Q_\lambda = \frac{I_\lambda}{F_\lambda} \qquad [2.2]$$

2.1. Data Quality Issues

2.1.1. SBUV/2 Wavelength Change. The BUV and SBUV instruments were designed with Channel 1 located at 255.7 nm. It was later realized that radiances at this wavelength could be contaminated by NO γ-band emission [*McPeters*, 1989]. The wavelength for Channel 1 was changed to approximately 252.0 nm for all SBUV/2 instruments. The predicted effect of NO emissions on Channel 1 radiances is small (< 2%). *Thomas et al.* [1991] nevertheless excluded these data in their analysis of Nimbus-7 SBUV measurements. We analyzed Nimbus-7 measurements both with and without 255.7 nm data, and found no qualitative difference in the results. We therefore include Channel 1 data in our Nimbus-7 SBUV analysis for consistency between all instruments.

2.1.2. Nimbus-7 SBUV Accelerated Deployment. Nimbus-7 SBUV normally made continuous scan solar irradiance measurements on one orbit per day, beginning near the Northern Hemisphere (NH) terminator (SZA ≈ 90°). For these orbits, the NASA V6 ozone processing algorithm omitted all descending node data (SZA > 72°). During selected periods in NH spring and summer (1980 days 198-324, 1981 days 183-261, 1984 days 139-204, 1986 days 177-219), Nimbus-7 solar measurements were made on every orbit to allow characterization of diffuser degradation [*Schlesinger and Cebula*, 1992; *DeLand and Cebula*, 2001]. As a result, no radiance data are available for SZA > 72° during these periods. No latitude coverage was lost, because the NH descending node data begin at the maximum latitude of 81°N and continue down to ~68°N. All data during accelerated deployment periods were omitted from the analysis of *Thomas et al.* [1991]. We used the limited SZA range data in our analysis, and found no differences in PMC statistical behavior between these accelerated deployment intervals and periods with full SZA coverage.

2.1.3. SBUV/2 Orbit Drift. The POES afternoon operational satellites are launched into sun-synchronous orbits with initial equator-crossing times of ~1400 UT. For NOAA-9, NOAA-11, and NOAA-14, the orbit drifted to later equator-crossing times with an initial rate of $\Delta t_{Eq} \approx 30$ minutes/year, increasing as the orbit neared the terminator (Figure 1). The orbits of NOAA-9 and NOAA-11 crossed the terminator after approximately 6 years, so that the second half of each instrument's data record represents morning equator-crossing times on the descending node of the orbit. Near-terminator measurements are problematic for PMC analysis because the data are compressed into a small SZA range at high SZA values. As a consequence of these effects, no results are presented here for NOAA-9 1990 Northern Hemisphere (NH), 1990-1991 SH, and NOAA-14 2001-2002 SH PMC seasons because of inconsistent behavior in the processed data. Beginning with NOAA-16, the orbit insertion of the POES afternoon spacecraft was revised to delay the onset of significant orbit drift by 4-5 years [*Price*, 1991]. Further discussion of the impact of orbit drift on SBUV/2 PMC results is given in Section 4.2.

2.1.4. SBUV/2 Grating Drive Errors. The grating drive system on early SBUV/2 instruments began to experience minor problems with wavelength selection after 4-5 years of operation. Errors of ±1-2 grating position (1 GPOS ≈ 0.074 nm) were frequently observed for NOAA-9 and NOAA-11. Corrections for these errors were applied during V6 processing, and are included in the Q-values on the archived PMFs [*Flynn et al.*, 2000]. NOAA-14 SBUV/2 had more severe grating drive problems due to particulate contamination in the bearings, requiring the Channel 5 wavelength value to be shifted from 292.3 nm to 295.0 nm in June 1998. This change is accounted for in our analysis.

2.1.5. SBUV/2 Out of Band Response. The terrestrial backscattered radiance increases by four orders of magnitude over the 252-340 nm wavelength range observed during normal SBUV/2 operations. Measurements at the shortest wavelengths are thus sensitive to out-of-band (OOB) contamination from long wavelength signals. While the SBUV/2 double monochromator optical design is very efficient at stray light rejection, inflight data for some instruments show errors up to 5-6% at 252 nm over bright surfaces [*Flynn et al.*, 2000]. This error has been characterized for each instrument as a function of surface reflectivity and solar zenith angle for each scene. The PMF data used for this work include the OOB correction as a component of the V6 processing.

3. PMC Detection Algorithm

The PMC detection algorithm used in this work follows the original technique developed by *Thomas et al.* [1991]. It takes advantage of the extremely low terrestrial albedo in the mid-UV, with a broad minimum due to ozone absorption centered at approximately 250 nm. Microphysical models of PMC formation restrict the size and composition of the particles believed to be present [*Jensen and Thomas*, 1988; *Rapp et al*., 2002]. Recently the particle composition has been definitely identified as water-ice [*Hervig et al*., 2001], at least for a brighter subset of PMC. Based on measurements of the angular scattering [*Thomas and McKay*, 1985] and recent multispectral lidar data [*von Cossart et al.*, 1999] and the microphysical models, we expect that a PMC will appear in SBUV/2 measurements as a spectrally dependent enhancement of the backscattered signal, with the maximum enhancement at the shortest wavelength. However, negative fluctuations in upper stratospheric ozone will also induce positive variations in backscattered ra-

diance. Random instrument noise can also mimic weak PMC. In order to identify the relatively faint PMC signature, we first characterize the background albedo in the polar region, defined as all data poleward of 50° latitude, by calculating a 4th order polynomial fit as a function of solar zenith angle (SZA) to all valid samples for a given day. It should be recognized that since all SBUV/2 measurements are made in the nadir, the scattering angle and the SZA are complementary angles. While other functional forms, such as terms of cos(SZA) could be used to approximate the angular dependence of the background radiance, the polynomial fit proved to be satisfactory. This step is performed for each of the five shortest wavelength channels (252.0-292.3 nm). We then subtract the background fit from the data, and apply a set of 4 tests to the residual albedo values, r_λ, to determine the presence of a PMC in a given scene.

1. $r_{252}, r_{273}, r_{283} > 0$.
The residuals for the three shortest wavelengths (252, 273, 283 nm) must all be positive.

2. $m_\lambda < 0$.
A linear regression fit to the five residuals as a function of wavelength is calculated. The slope, m_λ, of this regression fit must be negative.

3. $r_{252} > (\sigma_{252} * [\langle A_{252}\rangle_{bin}/A_{252}(81°)])$.
The 252 nm albedo values are separated into 10 bins over the SZA range for the current day, with an equal number of samples in each bin. The average albedo, $\langle A_{252}\rangle_{bin}$, and standard deviation, σ_{252}, are calculated for each bin. An average albedo at the maximum observed latitude (81°) is also calculated. The 252 nm residual must exceed a noise term defined by the product of the variability in the corresponding SZA bin and a scaling term relating the local albedo to the reference albedo.

4. $r_{252} > r_{273}$.
The 252 nm residual must be greater than the 273 nm residual.

For samples that pass these tests, we also require the 252 nm residual to exceed the smaller of either $7x10^{-6}$ (absolute value) or 5% of the background albedo value to reduce the occurrence of "false positive" PMC detections (see Section 3.2). We run the detection algorithm on each day's data for 5 iterations, excluding all samples identified as PMCs from the background fit for subsequent iterations. Figure 2(a) shows an example of 252 nm albedo data for NOAA-9 SBUV/2 on 1985 day 180. The SZA dependence of the albedo values is well-represented by the 4th order polynomial fit. The latitude values for the heavy tick marks show that ascending node data are observed at lower SZA values ($SZA_{asc} \leq 70°$), while descending node data are observed at comparable latitudes but much higher SZA. Figure 2(b) shows the corresponding albedo residuals when the background fit is subtracted. The samples that do not satisfy all PMC detection criteria are evenly distributed about zero residual, and well-distributed in SZA. Typical standard deviations for the rejected residuals are ±1.0-1.5% at low SZA, increasing to ±2-3% for SZA ≥ 70°.

3.1. Geographic Distribution

Figure 3 shows the geographic distribution of the NOAA-9 PMC hits for 1985 day 180 as identified in Figure 2. Each box represents a SBUV/2 field-of-view for a single scan, elongated

slightly along-track because of spacecraft motion during sampling of the five shortest wavelengths. The colors indicate the strength of the PMC residual at 252 nm. Observations by MSX indicate that the horizontal extent of PMCs can be up to 500-1000 km [*Carbary et al.*, 2000]. The likelihood of detecting a single cloud in consecutive SBUV/2 scans therefore depends on both the extent and orientation of the cloud. Some examples of contiguous detections can be seen in Figure 3 (*e.g.* Siberia [65-75°N, 110°E], Finland [70°N, 35°E]). Note that where fields of view are horizontally close at low latitudes, they represent ascending node measurements from one orbit and descending node measurements from another orbit separated in time by 10-14 hours. Multiple detections at such locations may indicate long-lived clouds or preferred formation locations for short-lived clouds.

It is clear from Figure 3 and the discussion in Section 2 that SBUV-type instruments can only measure PMCs for latitudes up to 81°, which excludes approximately 9 % of the total area poleward of 60°. Since the SME observations indicate that the PMC frequency increases with latitude (at least up to 85^{o}, the highest latitude observed), especially for the brightest PMCs [*Olivero and Thomas*, 1986; *Thomas and Olivero*, 1991], the total frequencies presented in this paper are somewhat lower than if the coverage went all the way to the poles. However, we note that stricter latitude limits apply to many other NLC and PMC data sets, including all of the passive ground-based measurements, which includes all of the historic record prior to satellite or lidar measurements. The *g*-distribution fit results presented in Section 4.3 show minimal slope changes when the maximum latitude is reduced to 75°, despite a factor of 3 reduction in the number of PMCs available. This gives us confidence that our results are representative of the entire PMC region.

3.2. False Positive

The PMC detection algorithm presented in Section 3 responds to enhanced radiances from the PMCs that can also be produced by natural variations in upper stratospheric ozone, or random measurement errors. It is therefore important to estimate what fraction of PMC detections represent "false positives" caused by ozone variations, or measurement errors. Examination of SBUV/2 data from periods well outside the normal PMC season (from thirty days prior to Summer Solstice to seventy days afterwards), when very few or no PMCs are expected, shows detection rates of 1% or less using the algorithm described in Section 3. The detection rate increases to 1-2% during Northern Hemisphere spring as a result of increased gravity wave activity. These results are consistent with other observations showing that PMCs are only observed during a well-defined season [*Olivero and Thomas*, 1986; *Thomas and Olivero*, 1989]. The use of two forms for the minimum accepted 252 nm residual enables the PMC detection algorithm to respond to variations in albedo with solar zenith angle. At low SZA, requiring $r_{252} > 7x10^{-6}$ selects valid PMCs with small relative enhancements (*e.g.* 2-3%). This is to be compared with the requirement of $r_{273} > 5x10^{-6}$ used by *Thomas et al.* [1991]. At SZA > 70°, the decrease in albedo means that very few PMCs can pass the same absolute brightness test. Changing the threshold value to $r_{252} > 5\%$ provides additional PMC detections in this region. This is important for SBUV/2 instruments, where the drifting satellite orbit leads to entire PMC seasons with SZA > 70°. A reduction in either residual limit produces a significant increase in the false-positive detection rate as indicated by the out of season detection rate.

4. SBUV/2 PMC Results

4.1. Individual Season

An important validation of the SBUV/2 PMC algorithm is to compare results with the thoroughly studied SME data set [*Thomas*, 1995]. SME observed more faint PMCs because the limb measurement is made against a dark background. *Thomas* [1995] estimated that Nimbus-7 SBUV could only observe clouds in the top 10-25% of the SME UVS instrument detection range. For the Southern Hemisphere comparison shown here, only those PMCs with limb scattering ratio (LSR) values greater than 15 were included to approximate the lower SBUV and SBUV/2 PMC detection sensitivity, where the LSR is the ratio of the scattered radiance from the PMC to the background Rayleigh scattering for the SME measurements. SME Northern Hemisphere data show similar behavior to SBUV and SBUV/2 measurements when filtered with a threshold of LSR > 6. A north/south difference in the threshold LSR for SME PMC data exists because SME Southern Hemisphere measurements were made in forward scattering, which gives a stronger response than the backward scattering measurements used in the Northern Hemisphere. Figure 4 shows SME, Nimbus-7 SBUV, and NOAA-9 SBUV/2 daily PMC occurrence frequency results for the Southern Hemisphere during the 1985-1986 season. Each data point represents a summation over latitudes between 50-82.5°. Because of differences in satellite measurement location and observation time for any individual day, it is appropriate to compare the instruments over a full PMC season. The SME data (Figure 4(a)) increase rapidly beginning ~20 days before solstice (S-20), reaching a frequency of approximately 15% by S+5 days. A peak value of 18% is reached at S+28 days, followed by a decrease to near-zero frequency after S+45 days. Similar seasonal behavior is observed when the full SME PMC data set is examined, strongly suggesting that the behavior of the brightest PMCs is representative of the whole PMC population. The corresponding Nimbus-7 SBUV data shown in Figure 4(b) follow a similar seasonal behavior, with a smoothed maximum frequency of ~13% and individual days reaching approximately 20%. The NOAA-9 SBUV/2 results for the 1985-1986 SH season, shown in Figure 4(c), are very similar in magnitude and temporal structure to both the SME and the Nimbus-7 SBUV results. This gives us confidence that the PMC detection algorithm presented in Section 3 gives consistent results when applied to data from different SBUV instruments.

We have also examined the latitude dependence of the PMC results from the SBUV/2 instruments. Figure 5 shows the smoothed PMC frequencies for Nimbus-7 and NOAA-9 in 5° latitude bands during the 1985 NH season. Virtually no detections of bright PMCs are observed below 60°N. In the 60-65° band, NOAA-9 does observe PMCs at a 5-10% rate, corresponding to 4-8 PMCs per day, whereas Nimbus-7 still sees almost no PMCs. This result is also observed in other coincident years (1986-1989). For higher latitude bands, there are differences in seasonal behavior between bands, but agreement in time dependence between instruments. The differences in frequency may be caused by differences in sampling location and time. A comparison with the latitude dependence in the SME measurements shows general agreement in the latitudinal and seasonal dependence, although SME observed significantly more PMCs at latitudes greater than 70°, which can be at least partially attributed to differences in sensitivity between SME and the SBUV instruments.

4.2. Long-Term PMC Behavior

The overlapping data sets available from multiple SBUV and SBUV/2 instruments allow us to examine a continuous record of PMC behavior covering more than 20 years. Figure 6 shows the PMC daily occurrence frequency averaged over all latitudes for all Northern Hemisphere seasons and all satellites from 1979 through 2001. The basic seasonal pattern shown in Section 4.1 is present in all cases, but with significant interannual variations in amplitude and structure. A seasonal PMC frequency curve from a single satellite will be influenced by local measurement time, satellite instrument sensitivity, and mesospheric temperature and dynamics. The agreement between different instruments for a single season is very good in some cases (*e.g.* 1987, 1994, 1996), and poorer in other cases (*e.g.* 1989, 2001). The results for NOAA-9 in 1989 and NOAA-14 in 2001 are affected by orbit drift, because all measurements are compressed into a small range of solar zenith angle. The functional fit for the background albedo is less accurate in such situations, reducing the ability to differentiate PMCs from ozone fluctuations. All of the SBUV/2 instruments normally observe short-term structure on time scales of a few weeks within a given season. While planetary waves could lead to these multiple-peaks, determination of the causes in the present PMC measurements is the topic of future research. *Kirkwood et al.* [2002] and *Kirkwood and Stebel* [2002] have found a strong correlation between ground observations of noctilucent clouds and the effects of planetary waves. The Northern Hemisphere seasons of 1979-1981 and 1990-1992 have significantly lower occurrence frequencies than other years. This result is linked to solar activity variations, and is discussed further in Section 4.4.

Figure 7 shows the daily PMC occurrence frequencies for all Southern Hemisphere seasons and all satellites from 1978-1979 through 2001-2002. Agreement between instruments is generally good, particularly in 2000-2001, where three separate frequency peaks are observed. Nimbus-7 SBUV SH frequency values are low from 1978-1979 through 1983-1984, and remain consistently lower than NOAA-9 SBUV/2 when data from both instruments are available. This is different from the NH situation, where the two satellites are in agreement during 1985-1987, then diverge during 1988-1989 as NOAA-9 data begin to be affected by orbit drift. We do not have an explanation for this result. NOAA-11 frequency values are approximately twice as high as NOAA-9 during 1993-1994, 1994-1995, and 1997-1998. Although the NOAA-11 orbit was close to the terminator during these seasons, the observed behavior is different from both NOAA-11 NH results and NOAA-9 results in both hemispheres for similar conditions.

4.3. g-Distribution Analysis

Analysis of long-term PMC variations from SBUV/2 data requires statistical parameters that can be compared between different instruments and different years. One obvious choice is the frequency of PMC occurrence over the entire season. However, the frequency values shown in Figures 6-7 are influenced by SBUV/2 orbit drift. While the NOAA-11 SH 1993-1994 frequency curve is a factor of 2 higher than the SH 1992-1993 curve from the same instrument, analysis shows that the vast majority of the additional PMC detections occur at low absolute residual values (r_λ = 2-7x10^{-6}). Similar behavior is observed for the NOAA-11 SH 1994-1995 and SH 1997-1998 seasons. For this reason it is desirable to use a parameter that is less sensitive to differences between individual SBUV/2 instruments or year-to-year variations in their equator crossing times.

The statistical distribution of PMC brightness, or albedo, is of fundamental importance in the study of PMC microphysics and in analyzing the interannual variability of the clouds. *Thomas* [1995] describes two specific quantities of interest: *f*, the frequency distribution, and *g*, the cumulative distribution. $f(r_\lambda)$ is defined as the number of clouds observed over a PMC season in a specified bin of residual albedo r_λ, observed at specified latitude intervals, divided by the total number of observing opportunities. A further division into longitudinal dependence is possible with sufficient statistics. In this paper, we limit the analysis to zonal averages. This treatment is justified by our own data, and by earlier studies based on SME data [*Thomas and Olivero*, 1989], showing that the longitudinal dependence of PMC appears to be quite weak in the seasonal average. The residual albedo r_λ is equivalent to the excess albedo A_n defined by *Thomas* [1995]. The cumulative distribution $g(r_\lambda)$ for a given albedo is then defined as the sum of the frequencies *f* over all higher albedo values. *Thomas* [1995] presents further detail and analytic approximations for *f* and *g* based on a physical model of temperature and/or water vapor fluctuations.

$$f_{SBUV} = \beta_n e^{-\beta_n r_\lambda} \qquad [4.1]$$

$$g(r_\lambda) = \int_{r_\lambda}^{\infty} f(r_\lambda')\,dr_\lambda' \qquad [4.2]$$

We employ the *g*-distribution exclusively in further discussion because it is inherently smoother. The *f*-distribution is derivable from *g* by differentiation. We chose an interval of the 252 nm albedo residual $r_\lambda(i)$ for the i-th bin of $1\text{x}10^{-6}$. Averages were calculated over all observed latitudes in the PMC region to improve the statistics. We parameterized the *g*-distribution for a given PMC season by calculating a linear regression fit to $\log_{10}(g(r_\lambda))$, using a range from $r_\lambda = 7\text{x}10^{-6}$ to the largest r_λ bin with 5 or more samples. The value of this maximum bin can vary from $15\text{x}10^{-6}$ to $35\text{x}10^{-6}$, depending most strongly on location in the solar activity cycle and brightness distribution within the season. Figure 8 shows that the dependence of $\log_{10}(g)$ versus r_λ is approximately linear for both hemispheres, in agreement with the earlier study of *Thomas* [1995] using Nimbus-7 SBUV data. The least-squares fit is usually quite good, with linear correlation $R > 0.995$. The distributions for some seasons were found to be non-linear in a portion of the albedo range, typically due to a few additional cloud identifications in a large- r_λ bin where the number of "hits" was small. These cases were identified by inspection, and the regression fit recalculated using only the linear section of the curve. The key results of the fit are the slope, β_n, whose inverse is a measure of the relative number of bright clouds to weak clouds, and the Y-intercept. Assigning a fixed maximum value for r_λ produces small changes in these values for a given season, but does not affect long-term results. Evaluating $g(r_\lambda)$ at the minimum threshold value ($r_\lambda = 7\text{x}10^{-6}$) gives the overall frequency of occurrence used in previous climatological studies of PMC [*Olivero and Thomas*, 1986; *Thomas and Olivero*, 1989]. We therefore choose to calculate a cumulative frequency for each PMC season using only PMCs with absolute residual values $r_\lambda(252\text{ nm}) \geq 7\text{x}10^{-6}$. This is consistent with the *g*-distribution linear fit region defined above. We also use the *g*-distribution regression slope β_n for each instrument and season as an indication of the PMC brightness distribution within that season. Smaller negative values of β_n indicate an increase in bright PMCs relative to fainter PMCs.

4.4. Correlation With Solar Activity

The abundance of water vapor in the 80-85 km region, where PMCs form, should be strongly affected by solar activity [*Garcia*, 1989]. Solar Lyman alpha (121.6 nm) radiation, which photodissociates H_2O, varies by almost a factor of two over an 11-year solar cycle [*Woods and Rottman*, 1997]. Direct measurements of Lyman α irradiance have not been made continuously throughout the past two solar cycles. However, *Woods et al.* [2000] used UARS SOLSTICE and SUSIM data to develop an improved proxy model of Lyman α variations based on different solar UV activity indices. Using 10.7 cm flux and Mg II index data to supplement direct irradiance measurements, they created a composite Lyman α irradiance data set covering the period 1947-1999 that can be used to evaluate PMC sensitivity to solar activity.

Figure 9 shows the PMC cumulative frequency values defined in Section 4.3 for all Northern Hemisphere seasons from 1979 through 2001. No normalization between different instruments has been applied. Solar activity is represented by the Lyman α irradiance from *Woods et al.* [2000], averaged over each PMC season (S–30 days to S+70 days) and scaled to fit on the plot. A clear anti-correlation between cloud frequency and solar activity is evident, consistent with the Nimbus-7 SBUV analysis shown by *Thomas et al.* [1991]. There is also a suggestion of a time lag between the frequency and solar activity values, which is consistent with the NLC analysis of *Gadsden* [1998] and of *Thomas and Olivero* [2001]. We have calculated multiple linear regression correlation coefficients from these data, averaging all available satellites for each season and using Lyman α irradiance and time as independent variables. PMC frequency lags were calculated in 0.5 year increments from –1.5 years to +1.5 years. The solar activity correlation coefficients for all lags are listed in Table 3. The highest correlation for Northern Hemisphere frequency values was found for τ_{lag} = +0.5 years, with R_{solar} = –0.87. The simultaneous linear regression with time gives R_{time} = 0.49. However, as can be seen in Table 3, the solar activity correlation varies irregularly with the phase lag and the uncertainty is about ±1 year. The solar activity correlation coefficient is highly significant for the 22 PMC seasons included in the fit. The positive trend correlation coefficient suggests an increase in cloud frequency with time, although the magnitude is not statistically significant. However, the cloud frequency values observed during the minimum between solar cycles 22 and 23 (1996, 1997) are substantially higher than those observed during the previous solar minimum (1985-1987). Figure 10 shows the cumulative PMC frequency results for Southern Hemisphere seasons from 1978-1979 through 2001-2002. The scaled solar activity values are averaged over corresponding SH seasons, and thus differ slightly from those shown in Figure 9. However, the overall solar cycle variation is not affected. The anti-correlation with solar activity is less obvious than the NH result during 1988-1993, but very pronounced during 1994-2000. The 2000-2001 season has an anomalously high frequency considering its location in the maximum of solar cycle 23, although all three active SBUV/2 instruments (NOAA-11, NOAA-14, NOAA-16) observed increased values. The maximum correlation coefficient for the SH data is found at τ_{lag} = 0.0 years (R_{solar} = –0.65, R_{time} = 0.51). The trend correlation is very similar to the NH result. The multiple regression fit parameters for the phase lags with the largest solar correlation coefficient are listed in Table 4.

The *g*-distribution regression slope values for all Northern Hemisphere PMC seasons are plotted in Figure 11. There is some anti-correlation between slope and solar activity for the maxima of solar cycles 21 and 22, suggesting that the PMC brightness distribution becomes steeper (fewer bright clouds) when solar activity is high. However, solar cycle 23 data do not yet

show a corresponding decrease. The multiple linear regression analysis gives maximum agreement for a lag of –0.5 years (R_{solar} = –0.63, R_{time} = 0.58). Southern Hemisphere *g*-distribution slope values are shown in Figure 12. The time dependence trend is much more pronounced in these data, as evidenced by the maximum correlation coefficients of R_{solar} = –0.60, R_{time} = 0.85 found at τ_{lag} = +1.0 years. The slope for the secular term of the multiple regression fit to the SH data listed in Table 4 is more than twice as large as the NH secular term. The positive values of the secular term means that the slopes of the g-distribution are becoming less negative with time, corresponding to an increase in the relative fraction of brighter PMCs within the seasonal distribution. This increase in the proportion of brighter clouds is much more pronounced in the Southern Hemisphere than in the Northern Hemisphere.

5. Discussion

5.1. Solar Cycle Effects

Until recently, there was no consensus on whether the solar cycle was present in long-term NLC records (see *Gadsden* [1998] for a review of this question). In the modern period for which higher-quality ground-based data have become available, there is a clear 11-year periodicity with more NLC sightings during solar cycle minimum [*Simmons and McIntosh*, 1983]. It has been speculated that the 11-year anti-correlation of NLC activity with the 10.7 cm solar radio flux is a result of the greater solar UV heating rate during solar maximum conditions (see *Gadsden* [1990, 1998] and references therein). *Garcia* [1989] first pointed out the importance of solar photodissociation for controlling the water vapor concentration, and thus the ice particle formation rate. Since the time constants for the heating rate (e.g. *Fritts and Luo* [1995]) and the photolysis rates are both short compared with a PMC season, the simple theory of solar forcing would thus predict maximum PMC brightness and activity during solar cycle minimum, and minimum PMC activity during solar maximum [*Thomas et al.*, 1991; *Thomas*, 1995]. However, *Gadsden* [1990; 1998] found that the maximum NLC frequency followed solar minimum by two years. This result was confirmed by *Thomas and Olivero* [2001] and found to be robust, with approximately the same time lag (±1 year) appearing in five different data sets. *Gadsden* [1998] found the best least-squares fit to the NLC cycle to be 10.3-10.5 years.

The results presented in this paper using 23 years of SBUV and SBUV/2 PMC data show that the highest correlation between solar Lyman alpha flux and PMC occurrence frequency is found for a time lag of approximately 0.5-1.0 year (solar activity leading PMC frequency). Changing the "best" value of τ_{lag} typically has a small effect on the derived correlation ($\Delta R \approx$ 0.01-0.05). Since the NLC time lag is uncertain by ±1 year, this result can be taken as confirmation of the results from the ground-based data set of NLC occurrences (number of NLC per season). The explanation for this remarkable effect is unknown. One possibility is that the stratospheric solar response is responsible. However, *Gadsden* [1998] showed that stratospheric temperature at 30 mb is essentially in phase with solar activity. Another possibility is that there is a significant time lag in mesospheric winds particularly in the upward wind which controls PMC growth through both temperature and water vapor [e.g. *Rapp et al.*, 2002]. *Gadsden* [1998] has shown that the available data for mesopause temperature in the 1964-1994 period [*von Zahn*, 1990] are inversely correlated to the annual NLC occurrence number, but only for the secular component, not the solar component. This is surprising in light of the apparent strong solar control of PMC/NLC. His result suggests that the mesopause temperature itself has no appreciable

solar-cycle dependence. This was borne out in a thorough study of *in situ* temperature measurements performed by falling spheres in the mid-1960s and in the last decade [*Lübken*, 2000]. Lübken found no solar cycle dependence in this data set, although this is not a very robust result because the majority of the data were collected during solar minimum conditions.

Recently, *Remsburg et al*. [2002] found a direct correlation between temperature and solar activity up to 80 km in HALOE data. Their analysis did not extend poleward of 40°. They observed an approximate 1-year time lag between the solar cycle index and the temperature which could not be explained. However, these results are only suggestive of a possible explanation of a phase in the PMC frequency relative to the solar cycle since they covered one solar-cycle and did not include either the altitudes or latitudes at which PMCs are measured. Much more information on the PMC environment is needed, particularly simultaneous data on PMC, temperature, and water vapor. The results presented in this paper clearly demonstrate agreement between PMC behavior and solar activity variations, but do not directly address the length of any periods in either data set.

5.2. Long-term Trends

As discussed in Section 4.4, after removing the solar-cycle anti-correlation, there is a weak increase in the frequency of PMCs in the NH over the past 23 years and a statistically significant increase in the proportion of the brighter PMCs in both hemispheres. These trends should be placed in context of other recent studies on possible secular increases in the frequency and the brightness of PMCs. *Thomas et al.* [1989] suggested that NLC are a recent phenomenon, appearing as a consequence of growing concentrations of methane (CH_4). Since CH_4 eventually oxidizes to water in the upper stratosphere and mesosphere, brighter and more frequent mesospheric clouds should occur with increased moisture, according to the model of *Jensen* [1989]. *Gadsden* [1985] first made the suggestion of a secular increase in the number of nights, N_{NLC}, that NLC are sighted. Further studies have quantified the long-term rate of increase using linear regression of the time series between 1964 and 1995, and including a cyclic component [*Gadsden*, 1990, 1998]. He found that although there has been no change of the seasonality, or the lower latitude boundary, the secular increase in N_{NLC} has been a factor of 2.6 over the 31-year period 1964-1995. Because of the nature of the function in the secular fit (a logistic curve), the vast majority of the change occurred before 1990. However, as *Gadsden* [1998] has pointed out, there may be a physical upper limit ($N_{NLC}/N_{total} \sim 0.5$) on the frequency of NLC. From this, it appeared that the secular increase has "saturated", and is not detectable in time series covering only the last decade.

Shettle et al. [2002a] recently analyzed three satellite data sets for PMC. They performed a careful intercomparison to exclude all other important effects (such as instrumental, solar and tidal effects), which might cause the PMC frequencies to differ between the various data sets. They concluded that the brightest PMC have increased in number from the 1983-1986 period to the 1993-1996 period, at least in the Southern Hemisphere. Recent work using a 16-year data set from the SAGE-II solar occultation experiment has demonstrated that there was also a significant Northern Hemisphere increase in the number of bright clouds, relative to the weaker clouds, from 1985 to 2000 [*Shettle et al.*, 2002b]. A Southern Hemisphere increase was also found, although of lesser significance.

What is the explanation for the apparent secular increase in the frequency of the brightest clouds? At least two candidate theories have been put forward in the literature. *Thomas et al.* [1989] proposed that increasing water vapor, due to a rising concentration of methane in the stratosphere and mesosphere, could cause the ice clouds to become substantially brighter over time. In the nineteenth century, the mesopause region may have been normally too dry to sustain visible NLC. However, toward the end of the century the growing levels of water vapor would have caused the brightness of the clouds to exceed that of the sky background. A variation on this scenario was offered by *Thomas* [1996], who proposed that as a result of both increasing CO_2 (which in the model of *Portmann et al.* [1995] predicted a gradual lowering of temperature) and increasing methane, the geographic region in which mesopause ice saturation could occur would slowly expand. This change would shift the low latitude NLC boundary from polar regions to more populated regions, in which NLC would be visible to more observers. Extrapolating to a doubling of CO_2 from its present concentration moves the NLC boundary to ~35° latitude in both hemispheres. This expansion would allow NLC to be visible to a significant fraction of the human race. 'Precursor' clouds have been sighted over the Rocky Mountains at historically low latitudes (as far south as 39°N) during the past three summers by both ground observers [*Wickwar et al.*, 2002; *Taylor et al.*, 2002] and by the SNOE satellite [*Merkel, private communication*, 2001].

The water vapor hypothesis has received new support recently, with the report of a nearly 2 parts per million (ppm) increase of stratospheric water vapor over the past 40 years [*Rosenlof et al*., 2001; *Oltmans et al.*, 2000]. Up to half of this trend can be explained by the increase in methane. There is apparently an additional unidentified mechanism that has allowed additional water vapor to cross the "cold trap" in the tropical regions over the past few decades [*Reid et al.*, 2000]. The increase in water vapor has not been constant over the past ten years, but has varied considerably [*Nedoluha et al.*, 1999; *Randel et al.*, 2000; *Nedoluha et al*., 2000], even dropping to nearly zero in the late 1990's. A further complication is that the analyzed stratospheric methane trends [*Randel et al.*, 2000] do not correlate well with the extensively measured ground-based trends of methane. Assuming continuity of total hydrogen with altitude, a 2 ppm increase in stratospheric water vapor would yield about 1 ppm increase at the mesopause [*Thomas et al.*, 1989; *Thomas and Olivero*, 2001; *Marsh*, 2001]. *Marsh* [2001] has found a 1 % per year rate of increase of water vapor in HALOE data in the lower mesosphere. Water vapor increases would be expected to increase the mean size of ice particles, and since the brightness of such particles varies as r^6, only small increases in the radius, r, would be necessary to explain significant changes in the NLC brightness. *Gadsden* [1990, 1998] has criticized the idea that NLC have appreciably brightened during the time in which systematic observations have been made. He argued that if long-term brightening has taken place, the first appearance of NLC during evening twilight would occur at earlier times, since they would compete more and more efficiently with the background illumination of the twilight sky. However, there is observational evidence that NLCs have become progressively brighter over an observing site near Moscow [*Romejko et al.* 2002]. *Klostermeyer* [2002] recently reanalyzed the northwest Europe NLC data and concluded that NLC brightness increased by a factor of 5 between 1964-1974 and 1985-1994.

The second candidate explanation for the secular increase of NLC is that the mesopause temperature has decreased with time, expected from rising CO_2 levels and the general cooling of the upper atmosphere. Since the mesopause temperature minimum is the location where most of

the ice particles are nucleated, and the rate of creation of new particles depends very sensitively upon temperature, this would appear to be a plausible connection. However, a test of this hypothesis revealed no apparent correlation between the conditions at the mesopause and the occurrence of NLC's below [*Lübken et al*., 1996]. They speculated that this may be due to the fact that the wind direction changes between the mesopause (~88 km) and the NLC region (~83 km), and the air masses at the two different altitudes originated from two different locations. It is possible that the mesopause temperature can only be correlated with PMC/NLC when comparing with large horizontal spatial scales, typical of satellite measurements. *Gadsden* [1990] estimated that a change in mesopause temperature of –6 K was needed over the 1964-1989 time span to explain the large secular increase of NLC. This temperature change is much higher than predicted by models [e.g. *Akmaev and Fomichev*, 2001], but is not unreasonable compared with other trend estimates in the middle mesosphere [e.g. *Taubenheim et al.*, 1997]. *Lübken* [2000] has shown that *in situ* falling-sphere measurements fail to show any detectable trend in the summertime mesosphere over northern Scandinavia. These measurements span the period mid-1960 through the present. Thus it appears that we must look elsewhere to explain the large secular increases in NLC, and the smaller, but still significant, changes in the brighter PMC numbers. A complete understanding of long-term changes in PMC behavior requires more sophisticated models to explain both changes in cloud brightness and intensity-dependent changes in occurrence frequency.

6. Conclusion

We have shown that the SBUV series of instruments provides comprehensive geographic and temporal coverage of PMC behavior for the brightest portion of the PMC population. The combined SBUV and SBUV/2 PMC data set now extends over 23 years, and is expected to continue for at least another decade. These data verify the inverse relationship between PMC occurrence frequency and solar activity, previously observed only in the NLC time series. Stronger anti-correlation values are observed in the Northern Hemisphere ($R_{solar} = –0.87$). While there is a weak indication of a possible phase lag, the uncertainty is such that we can not distinguish between no phase lag and a 1.5 year phase lag. The SBUV PMC data also suggest a secular increase in the relative proportion of the brightest clouds within the overall population. This may be a result of water vapor increases which tend to enlarge the ice particle size. The trend is considerably stronger in Southern Hemisphere data ($R_{time} = +0.85$). Further work will take advantage of overlapping data from different SBUV/2 instruments to examine local time, inter-annual, and inter-hemispherical variations in PMC behavior. We also plan to analyze the SBUV/2 continuous scan data, where Earth view radiance spectra covering the 200-400 nm wavelength region are collected for part of a day.

7. Acknowledgements

This research was primarily supported by NASA's Office of Space Science. Portions of G. E. Thomas' time were supported by the Aeronomy Program of the National Science Foundation. Portions of E. P. Shettle's time were also supported by the Naval Research Laboratory. The SBUV/2 data were obtained from NOAA/NESDIS with support from the NOAA Climate and Global Change Atmospheric Chemistry Element. We would like to thank Dr. R. McPeters for his helpful comments on this research.

Table 1
SBUV/2 Instrument Observations

Instrument	*Launch Date*	*Data Available for PMC Analysis*	*Comments*
Nimbus-4 BUV	4/4/1970	Apr 1970 - Jul 1972	Questionable data quality near SAA.
Nimbus-7 SBUV	10/31/1978	Nov 1978 - Jun 1990	Non-sync correction applied after Feb 1987.
NOAA-9 SBUV/2	12/12/1984	Mar 1985 - Feb 1998	Terminator crossing fall 1990. Missing data: Aug 1993, Aug 1995, May-Jun 1996. Data collection reduced to 4 orbits/day after Jul 1997.
NOAA-11 SBUV/2	9/24/1988	Dec 1988 - Apr 1995 Jul 1997 - Mar 2001	No data collected Apr 1995 – Jul 1997. Terminator crossing late 1995. Measurements reduced to total ozone wavelengths only beginning Apr 2001.
NOAA-14 SBUV/2	12/30/1994	Jan 1996 - Sep 2001	Data for Feb-Dec 1995 not currently processed. Operational data do not use Channel 3 (283.1 nm). Terminator crossing occurred May 2002.
NOAA-16 SBUV/2	9/21/2000	Oct 2000 - present	Current NOAA operational instrument.

Table 2
Standard SBUV/2 Wavelengths

Channel	*Nominal Wavelength* [nm]
1	252.0
2	273.6
3	283.1
4	287.6
5	292.3
6	297.5
7	301.9
8	305.8
9	312.5
10	317.5
11	331.2
12	339.8

Table 3
Correlation Coefficients vs. Solar Activity and Time

Solar Activity Lag [years]	NH Occurrence Frequency	SH Occurrence Frequency	NH g-distribution Slopes	SH g-distribution Slopes
–1.5	–0.31	–0.32	–0.34	–0.35
–1.0	–0.44	–0.49	–0.33	–0.48
–0.5	–0.68	–0.64	**–0.63**	–0.48
0.0	–0.75	**–0.65**	–0.55	–0.57
0.5	**–0.87**	–0.59	–0.60	–0.45
1.0	–0.85	–0.63	–0.57	**–0.60**
1.5	–0.83	–0.56	–0.62	–0.49
Correlation *vs*. time	0.49	0.51	0.58	0.85

The maximum correlation coefficient observed for each parameter is shown in bold.

Table 4
Multiple Linear Regression Fit Parameters

Parameter	Solar Coefficient	Secular Coefficient	Constant
NH Occurrence Frequency	–2.20(±0.32)	0.0650(±0.0403)	–114
SH Occurrence Frequency	–1.31(±0.43)	0.0951(±0.0550)	–180
NH g-distribution Slope	–0.288(±0.114)	0.0341(±0.0145)	–69.3
SH g-distribution Slope	–0.282(±0.098)	0.0817(±0.0125)	–164

Parameter = Coefficient(solar)*$F_{\text{Lyman alpha}}$ + Coefficient(secular)*t[years] + Constant

Lyman alpha flux values divideded by 10^{11} photons/cm^2/sec for fit calculations.

g-distribution slopes divided by 10^{-5} for fit calculations.

Figures

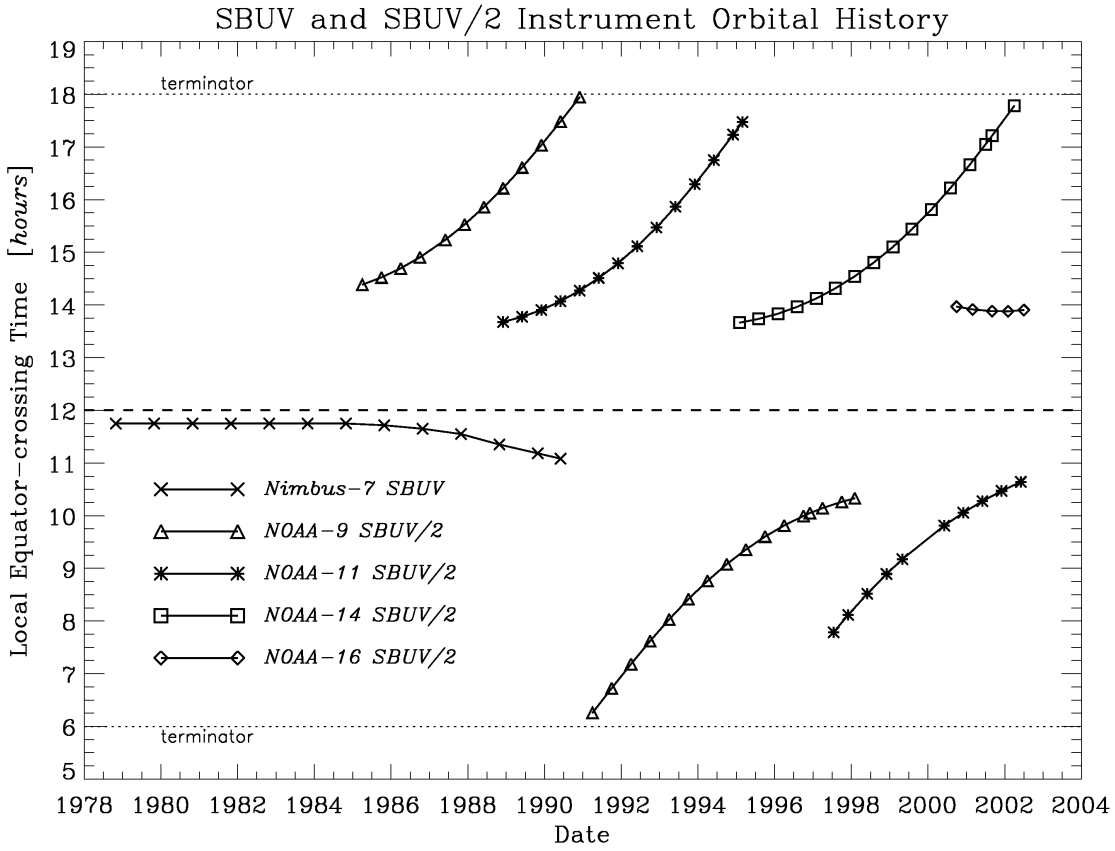

FIGURE 1. Time history of equator-crossing times for SBUV and SBUV/2 instruments. Measurements transition from ascending node (afternoon) to descending node (morning) when an instrument's orbit crosses the terminator.

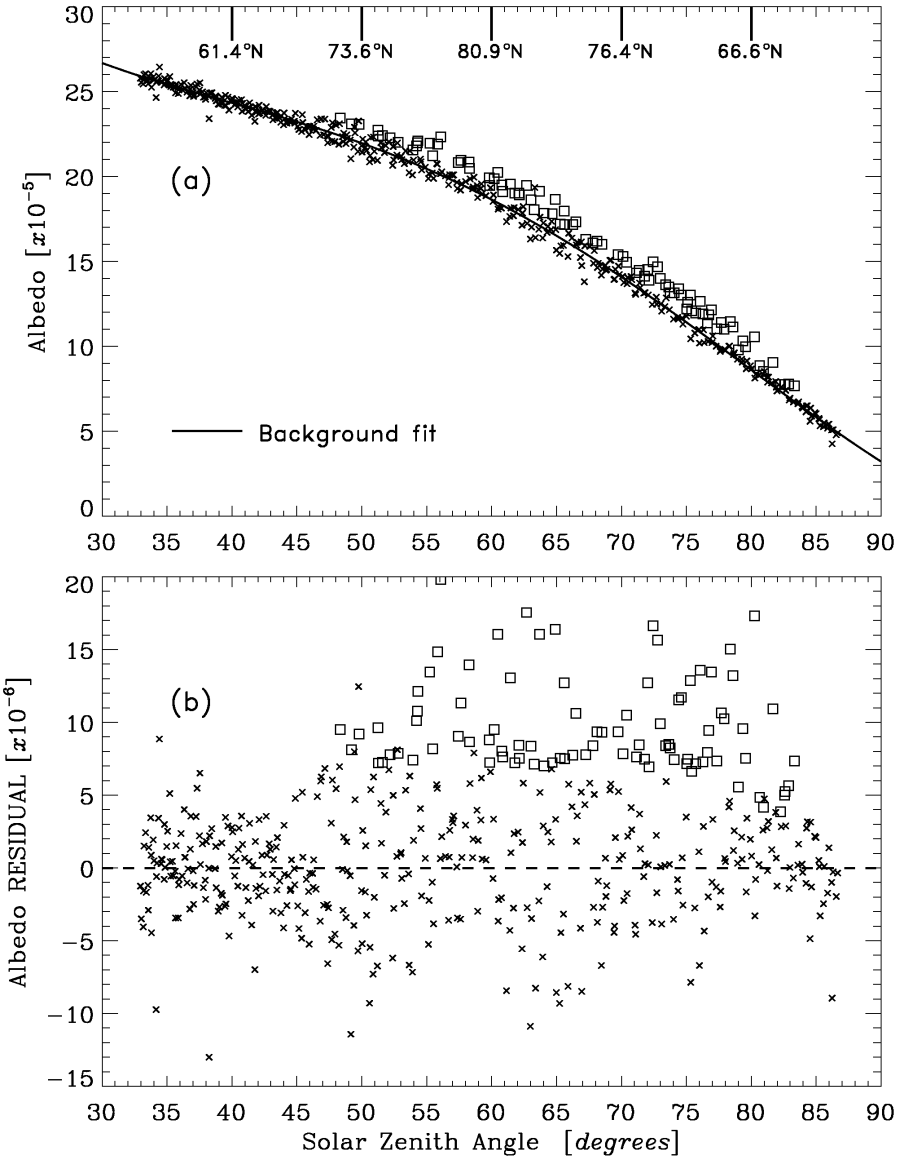

FIGURE 2. (*a*) NOAA-9 SBUV/2 252 nm albedo values for all measurements northward of 50°N on 1985 day 180. Squares indicate measurements identified as PMCs by the detection algorithm. The solid line is a 4th order polynomial fit to all non-PMC measurements. Heavy tick marks show approximate latitudes corresponding to reference solar zenith angle values. (*b*) 252 nm albedo residuals (data – fit) for the measurements shown in panel (*a*). PMC detections are indicated by squares.

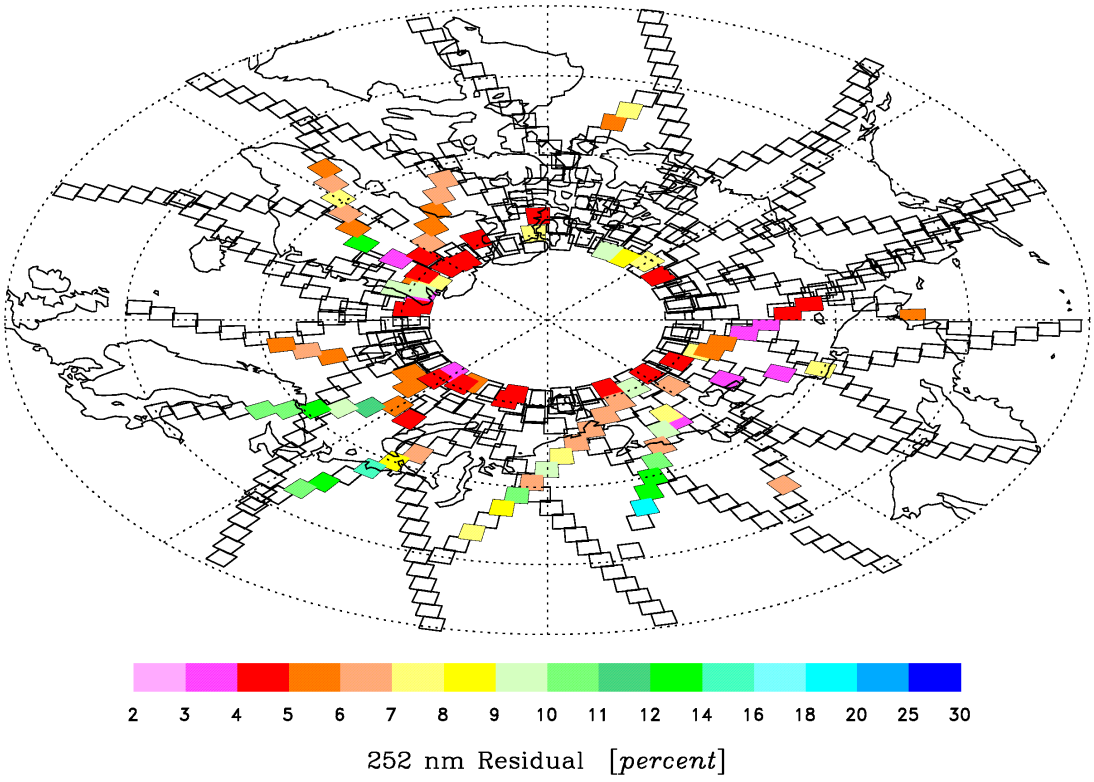

FIGURE 3. Geographic distribution of NOAA-9 SBUV/2 PMC detections for 1985 day 180. The plot range is 50°N-90°N. Each square represents an SBUV/2 field of view during the 10 seconds required to sample the 5 wavelengths used in the PMC detection algorithm. The intensity of each PMC detection is indicated by the color scale at the bottom of the figure.

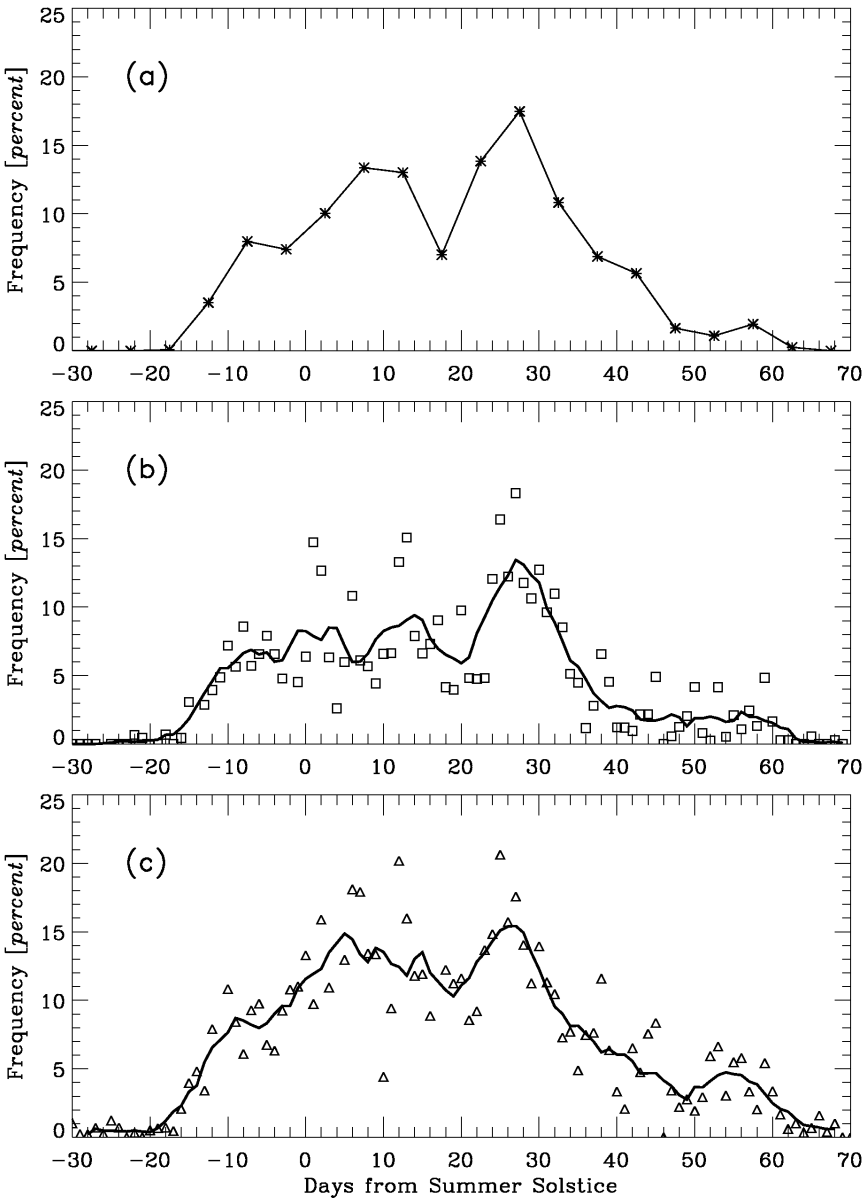

FIGURE 4. PMC frequency values in percent, summed over latitudes between 50°S-82.5°S for the Southern Hemisphere 1985-1986 season. The time coordinate is days from the summer solstice (1985 day 172). (*a*) SME data with LSR > 15, averaged in 5-day bins. (*b*) Nimbus-7 SBUV data. Squares are daily values, and the solid line is a 7-day running average. (*c*) NOAA-9 SBUV/2 data. Triangles are daily values, and the solid line is a 7-day running average.

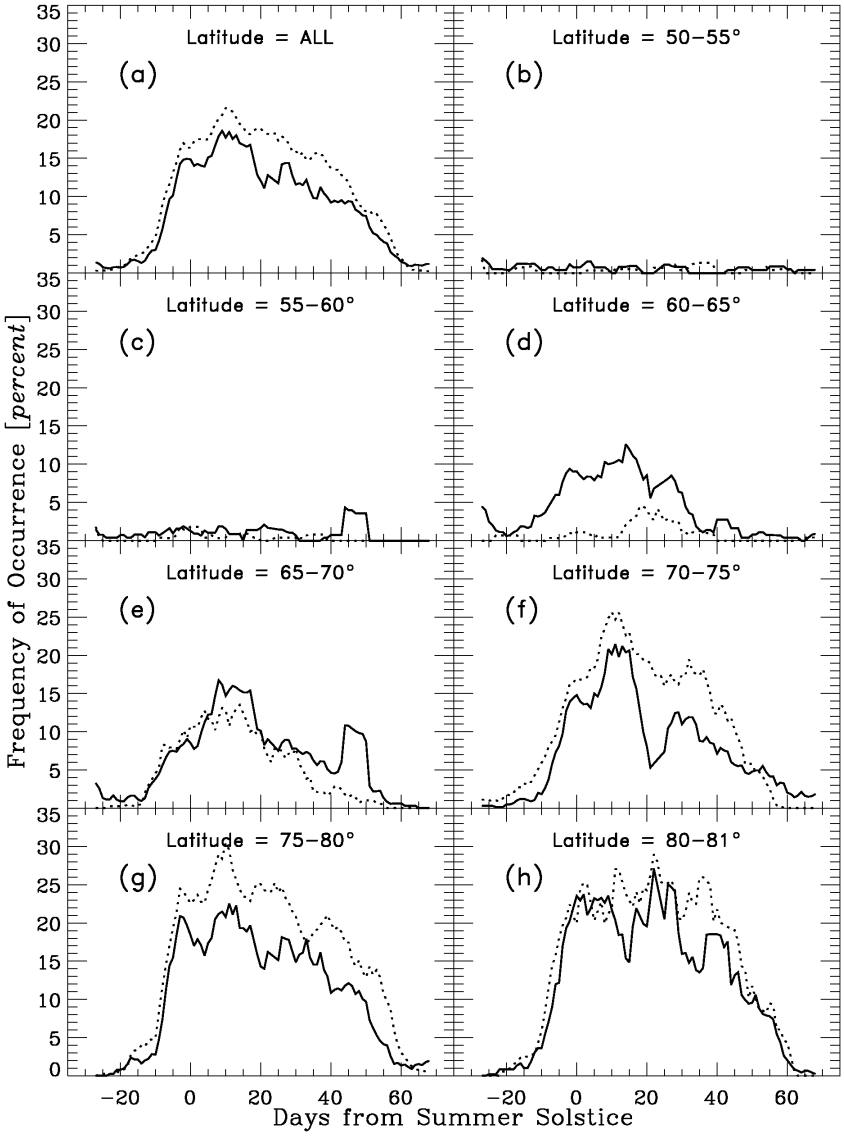

FIGURE 5. PMC frequency latitude dependence for the 1985 Northern Hemisphere season. Panel (*a*) is a summation over all latitudes. Panels (*b*)-(*h*) show frequency results for successive 5° latitude bands, beginning with 50°-55°N. Nimbus-7 SBUV results are shown as a dotted line, and NOAA-9 SBUV/2 results are shown as a solid line. All curves are 7-day running averages.

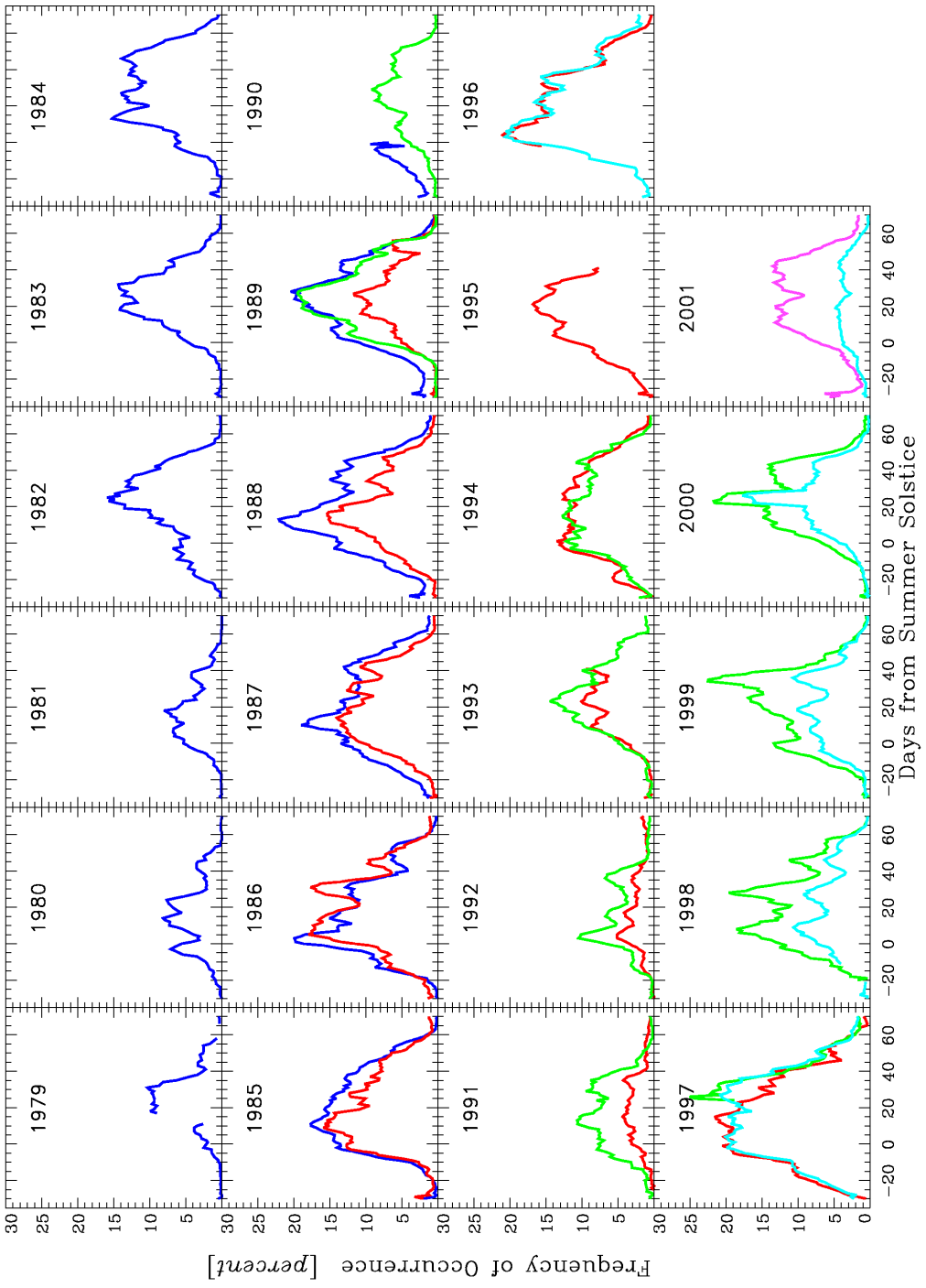

FIGURE 6. PMC frequency values for Northern Hemisphere seasons from 1979 to 2001. Nimbus-7 SBUV = *dark blue*, NOAA-9 SBUV/2 = *red*, NOAA-11 SBUV/2 = *green*, NOAA-14 SBUV/2 = *light blue*, NOAA-16 SBUV/2 = *magenta*. All curves are 7-day running averages.

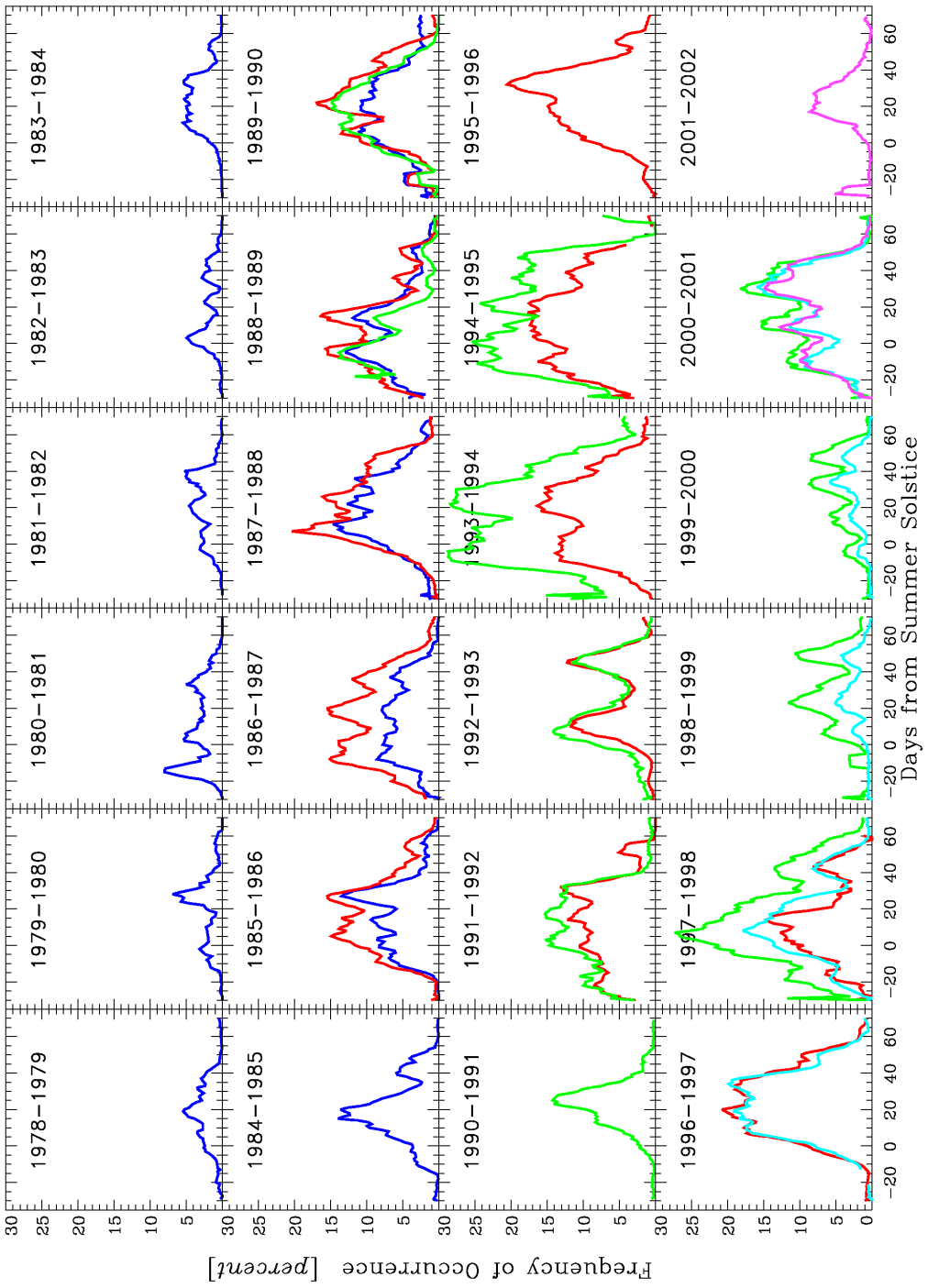

FIGURE 7. PMC frequency values for Southern Hemisphere seasons from 1978-1979 to 2001-2002. All curve identifications are as in Figure 6.

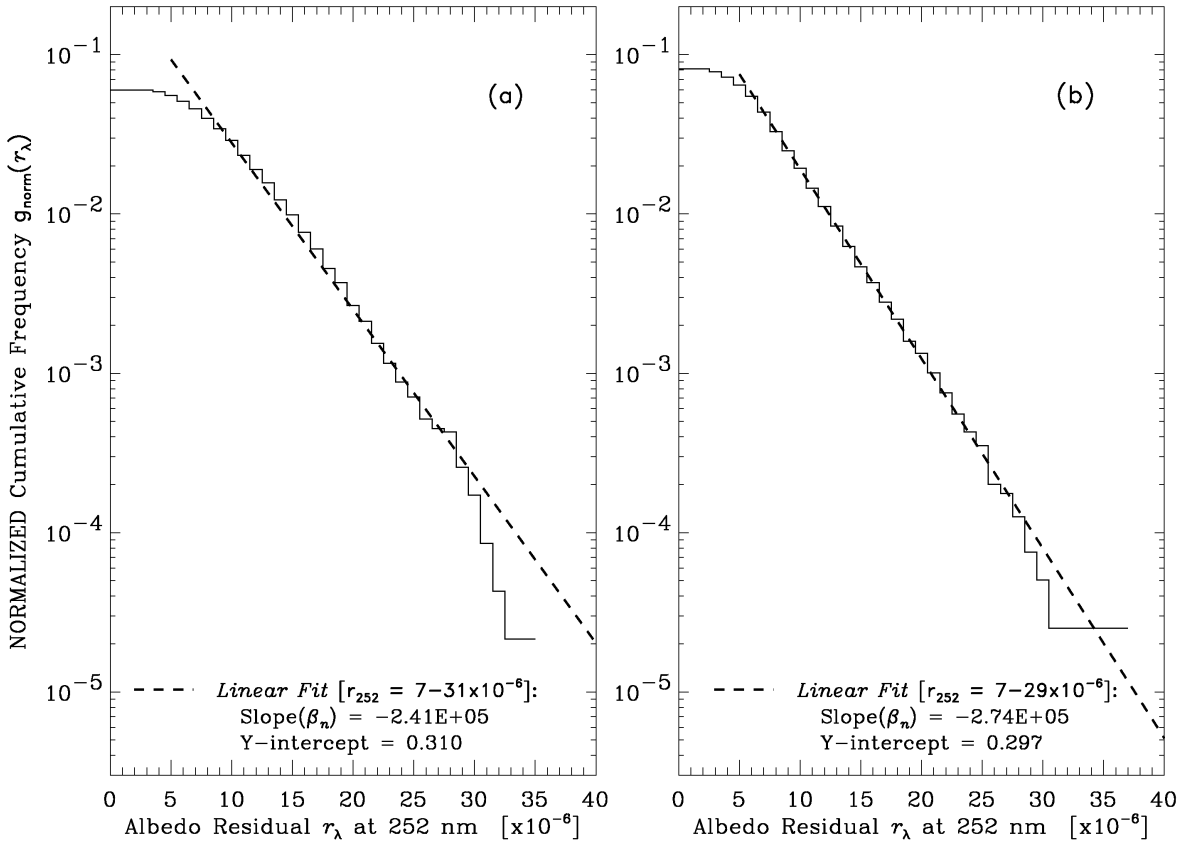

FIGURE 8. NOAA-9 SBUV/2 PMC frequency g-distribution plots: (*a*) 1986 Northern Hemisphere season; (*b*) 1986-1987 Southern Hemisphere season. The dashed line in each panel is a semi-logarithmic linear regression fit to the range of 252 nm residual values indicated in brackets.

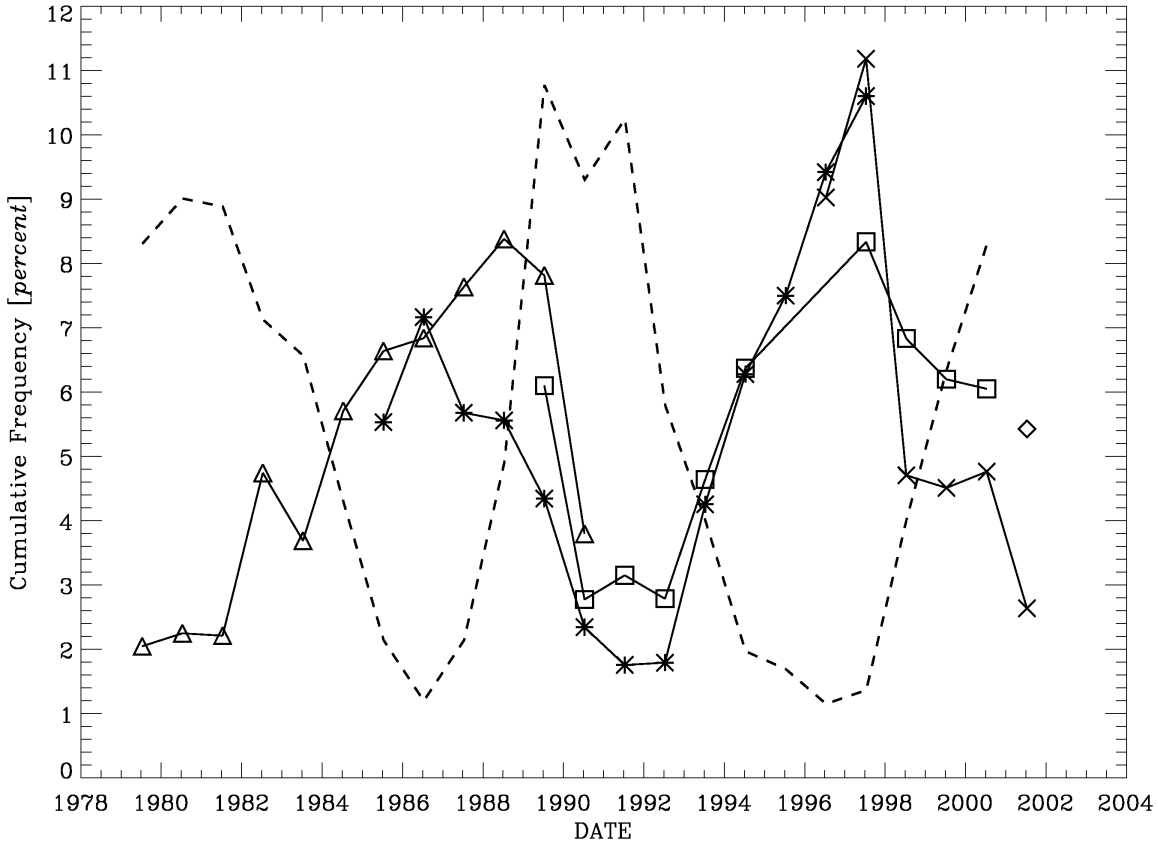

FIGURE 9. Time dependence of cumulative PMC frequency for each season from SBUV and SBUV/2 instruments for the Northern Hemisphere, using only measurements with $r_\lambda(252\ nm) \geq 7x10^{-6}$. Nimbus-7 SBUV = *triangle*, NOAA-9 SBUV/2 = *asterisk*, NOAA-11 SBUV/2 = *square*, NOAA-14 SBUV/2 = *cross*, NOAA-16 SBUV/2 = *diamond*. The dashed line shows Lyman α irradiances from *Woods et al.* [2000] averaged over each corresponding NH season, scaled to fit on the plot.

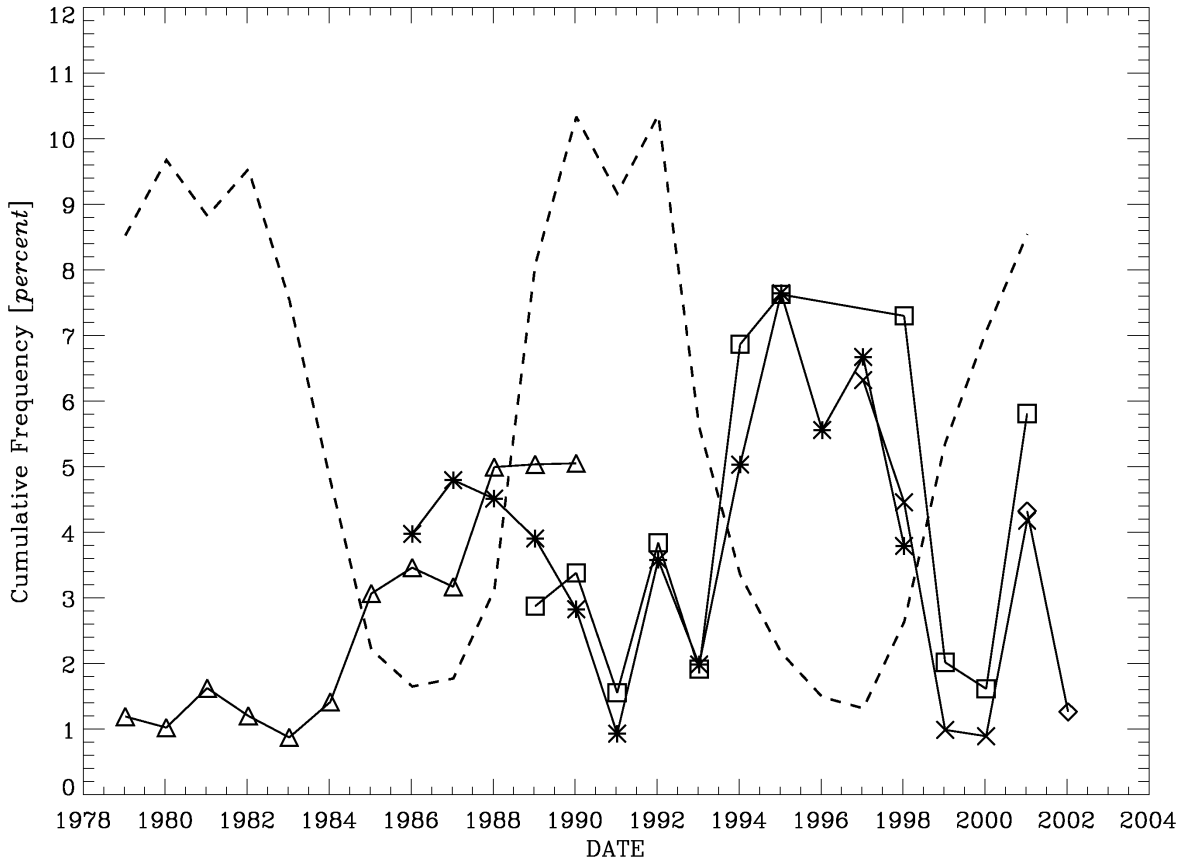

FIGURE 10. Time dependence of cumulative PMC frequency for each season from SBUV and SBUV/2 instruments for the Southern Hemisphere. All curve identifications are as in Figure 9. Solar irradiance values are scaled over corresponding Southern Hemisphere seasons.

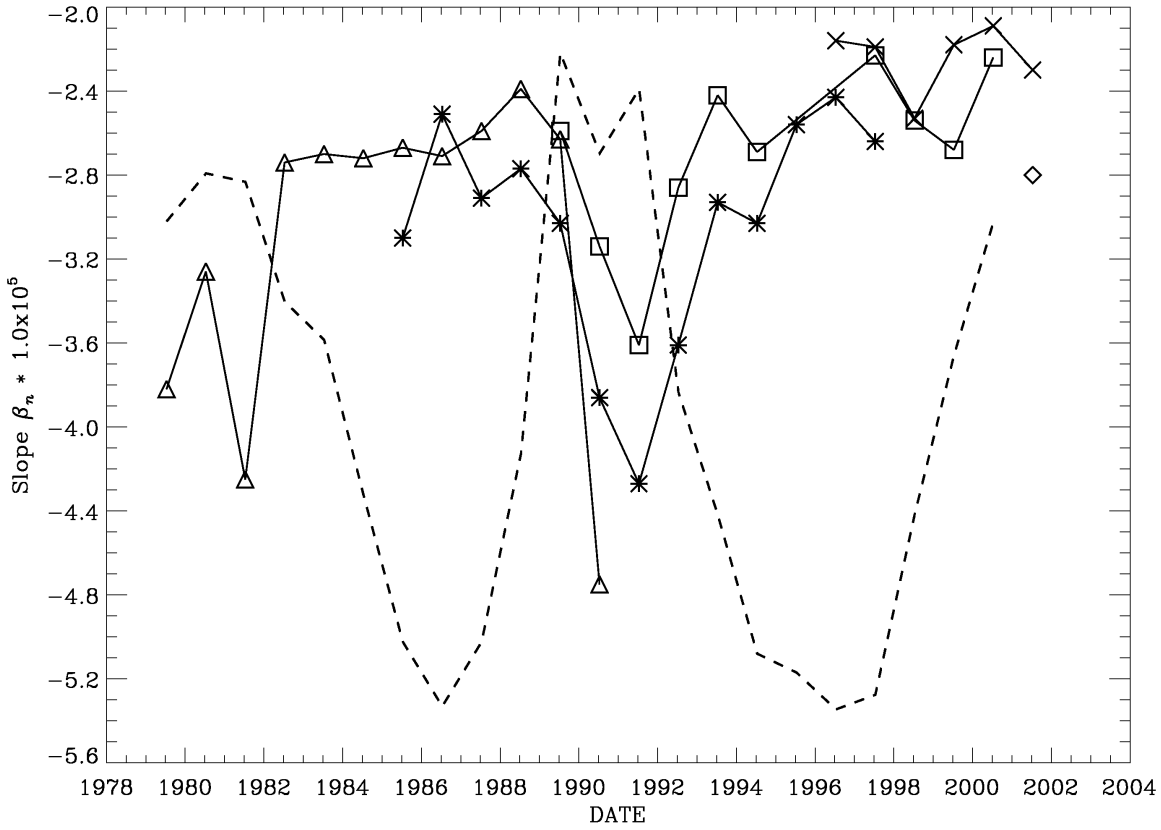

FIGURE 11. Time dependence of PMC g-distribution regression slopes from SBUV and SBUV/2 instruments for the Northern Hemisphere. All curve identifications are as in Figure 9.

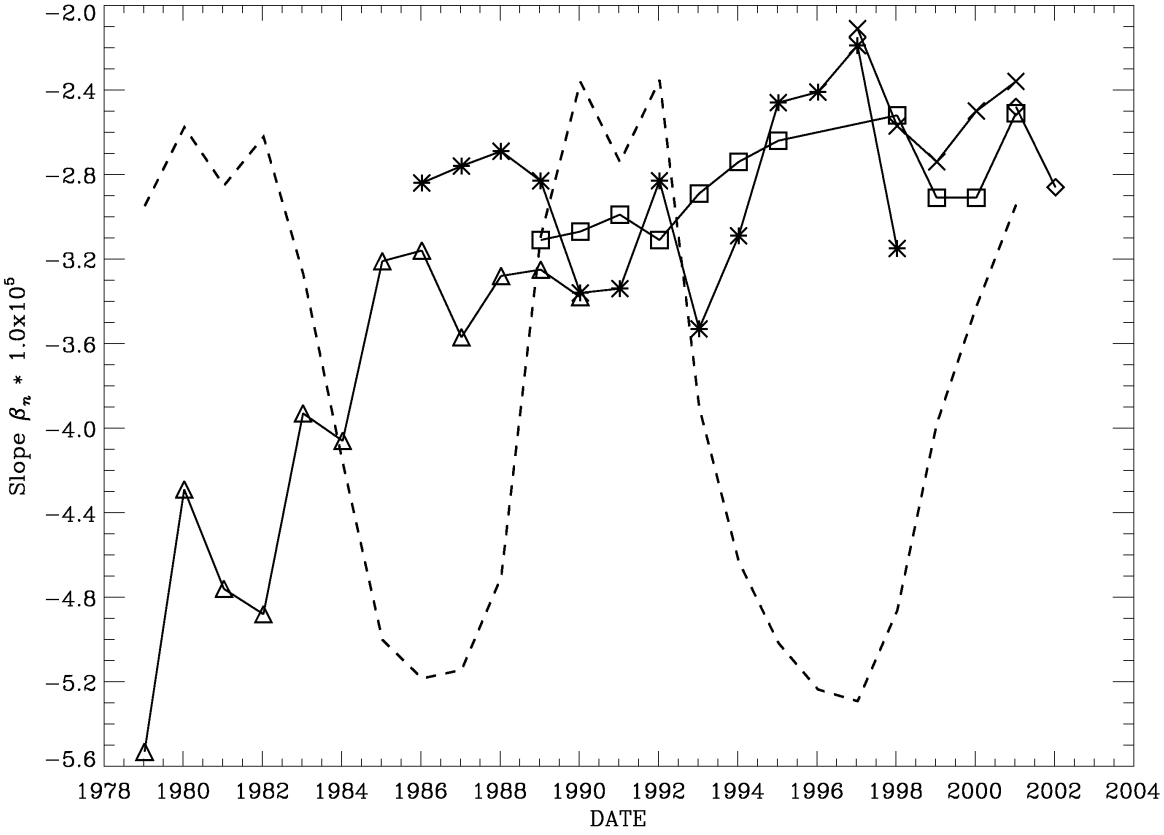

FIGURE 12. Time dependence of PMC g-distribution regression slopes from SBUV and SBUV/2 instruments for the Southern Hemisphere. All curve identifications are as in Figure 9.

References

Ahmad, Z., M. T. DeLand, R. P. Cebula, H. Weiss, C. G. Wellemeyer, W. G. Planet, J. H. Lienesch, H. D. Bowman, A. J. Miller, and R. M. Nagatani, Accuracy of total ozone retrieval from NOAA SBUV/2 measurements: Impact of instrument performance, *J. Geophys. Res., 99*, 22,975-22,984, 1994.

Akmaev, R. A., and V. I. Fomichev, A model estimate of cooling in the mesosphere and lower thermosphere due to CO_2 increase over the last 3-4 decades, *Geophys. Res. Lett., 27*, 2113-2116, 2000.

Bailey, S. M., G. E. Thomas, and A. W. Merkel, The climatology of polar mesospheric clouds from the Student Nitric Oxide explorer, *Eos. Trans. AGU, 82*(20), Spring Meeting Suppl., Abstract SA31B-05, 2001.

Bhartia, P. K., R. D. McPeters, C. L. Mateer, L. E. Flynn, and C. Wellemeyer, Algorithm for the estimation of vertical ozone profile from the backscattered ultraviolet technique, *J. Geophys. Res., 101*, 18,793-18,806, 1996.

Burton, S. P. and L. W. Thomason, Polar mesospheric clouds in SAGE II Version 6.0 Data, *Proc. Quadrennial Ozone Symp.*, Sapporo, Japan, Int. Ozone Comm., pp. 325-326, 3-8 July 2000.

Carbary, J. F., D. Morrison, and G. J. Romick, Transpolar structure of polar mesospheric clouds, *J. Geophys. Res., 105*, 24,763-24,769, 2000.

Carbary, J.-F., G. J. Romick, D. Morrison, L. J. Paxton, and C. I. Meng, Altitudes of polar mesospheric clouds observed by a middle ultraviolet imager, *J. Geophys. Res., 104*, 10,089-10,100, 1999.

Debrestian, D. J., J. D. Lumpe, E. P. Shettle, R. M. Bevilacqua, J. J. Olivero, J. S. Hornstein, W. Glaccum, D. W. Rusch, and M. D. Fromm, Preliminary analysis of Southern Hemisphere POAM II observations of polar mesospheric clouds, *J. Geophys. Res., 102*, 1971-1981, 1997.

DeLand, M. T., and R. P. Cebula, Spectral solar UV irradiance data for cycle 21, *J. Geophys. Res., 106*, 21,569-21,583, 2001.

DeLand, M. T., R. P. Cebula, L. K. Huang, S. L. Taylor, R. S. Stolarski, and R. D. McPeters, Observations of "hysteresis" in backscattered ultraviolet ozone data, *J. Atmos. Oceanic Technol., 18*, 914-924, 2001.

Donahue, T. M., B. Guenther, and J. E. Blamont, Noctilucent clouds in daytime: Circumpolar particulate layers near the summer mesopause, *J. Atmos. Sci., 30*, 515-517, 1972.

Evans, W. F. J., L. R. Laframboise, K. R. Sine, R. H. Wiens and G. G. Shepherd, Observation of polar mesospheric clouds in summer, 1993 by the WINDII instrument on UARS, *Geophys. Res. Lett., 22*, 2793-2796, 1995.

Flynn, L. E., S. Kondragunta, K. Horvath, and E. Beach, Internal validation of SBUV/2 ozone vertical profile data sets, *Proc. Quadrennial Ozone Symp.*, Sapporo, Japan, Int. Ozone Comm., pp. 75-76, 2000.

Frederick, J. E., R. P. Cebula, and D. F. Heath, Instrument characterization for the detection of long-term changes in stratospheric ozone: An analysis of the SBUV/2 radiometer, *J. Atmos. Oceanic Technol., 3*, 472-480, 1986.

Fritts, D. C. and Z. Luo, Dynamical and radiative forcing of the summer mesopause circulation and dynamical structure 1. Mean solstice conditions, *J. Geophys. Res., 100*, 3119-3128, 1995.

Gadsden, M., The North-West Europe data on noctilucent clouds: a survey, *J. Atmos. Terr. Phys., 60*, 1163-1174, 1998.

Gadsden, M. A secular change in the noctilucent cloud occurrence, *J. Atmos. Terr. Phys., 52*, 247-251, 1990.

Gadsden, M., Observations of noctilucent clouds from North-West Europe, *Annales Geophys., 3*, 119-126, 1985.

Garcia, R. R., Dynamics, radiation, and photochemistry in the mesosphere: Implications for the formation of noctilucent clouds, *J. Geophys. Res., 94*, 14,605-14,615, 1989.

Gleason, J. F., and R. D. McPeters, Corrections to the Nimbus 7 solar backscatter ultraviolet data in the "nonsync" period (February 1987 to June 1990), *J. Geophys. Res., 100*, 16,873-16,877, 1995.

Heath, D. F., C. L. Mateer, and A. J. Krueger, The Nimbus-4 Backscattered Ultraviolet (BUV) atmospheric ozone experiment - Two years' operation, *Pure Appl. Geophys., 106-108*, 1238-1253, 1973.

Heath, D. F., A. J. Krueger, H. A. Roeder, and B. D. Henderson, The Solar Backscatter Ultraviolet and Total Ozone Mapping Spectrometer (SBUV/TOMS) for Nimbus G, *Opt. Eng., 14*, 323-331, 1975.

Hervig, M., R. E. Thompson, M. McHugh, L. L. Gordley, J. M. Russell III, M. E. Summers, First confirmation that water ice is the primary component of polar mesospheric clouds, *Geophys. Res. Lett., 28*, 971-974, 2001.

Hilsenrath, E., R. P. Cebula, M. T. DeLand, K. Laamann, S. Taylor, C. Wellemeyer, and P. K. Bhartia, Calibration of the NOAA 11 SBUV/2 ozone data set from 1989 to 1993 using in-flight calibration data and SSBUV, *J. Geophys. Res., 100*, 1351-1366, 1995.

Jensen, E., A numerical model of polar mesospheric cloud formation and evolution, Ph. D. thesis, Univ. of Colorado, Boulder, 176 pp., 1989.

Jensen, E. J., and G. E. Thomas, A growth-sedimentation model of polar mesospheric clouds, *J. Geophys. Res., 93*, 2461-2473, 1988.

Kirkwood, S., V. Barabash, B. U. E. Brändström, A. Moström, K. Stebel, N. Mitchell, and W. Hocking, Noctilucent clouds, PMSE and 5-day planetary waves: A case study, *Geophys. Res. Lett., 29*(10), 10.1029/2001GL014022, 2002.

Kirkwood, S. and K. Stebel, The influence of planetary waves on noctilucent cloud occurrence over NW Europe, *to be published in J. Geophys. Res.*, 2002.

Klenk, K. F., P. K. Bhartia, A. J. Fleig, V. G. Kaveeshwar, R. D. McPeters, and P. M. Smith, Total ozone determination from the Backscattered Ultraviolet (BUV) experiment, *J. Appl. Meteor., 21*, 1672-1684, 1980.

Klostermeyer, J., Noctilucent clouds getting brighter, *J. Geophys. Res., 107*(D14), 10.1029/2001JD001345, 2002.

Krueger, A. J., D. F. Heath, and C. L. Mateer, Variations in the stratospheric ozone field inferred from Nimbus satellite observations, *Pure Appl. Geophys., 106-108*, 1254-1263, 1973.

Lübken, F.-J., Nearly zero temperature trend in the polar summer mesosphere, *Geophys. Res. Lett., 27*, 3603-3606, 2000.

Lübken, F.-J., Thermal structure of the Arctic summer mesosphere, *J. Geophys. Res., 104*, 9135-9149, 1999.

Lübken, F.-J., K.-H. Fricke and M. Langer, Noctilucent clouds and the thermal structure near the Arctic mesopause in summer, *J. Geophys. Res., 101*, 9489-9508, 1996.

Marsh, D. R., Trends in mesospheric ozone and interactions with water vapor trends in the atmosphere, paper presented at the Second Workshop “Long-term changes and trends in the atmosphere”, Prague, Czech Republic, 2-6 July 2001.

Mateer, C. L., D. F. Heath, and A. J. Krueger, Estimation of total ozone from satellite measurements of backscattered ultraviolet Earth radiance, *J. Atmos. Sci., 28*, 1307-1311, 1971.

McPeters, R. D., Climatology of nitric oxide in the upper stratosphere, mesosphere, and thermosphere: 1976 through 1986, *J. Geophys. Res., 94*, 3461-3472, 1989.

McPeters, R. D., The behavior of ozone near the stratopause from two years of BUV observations, *J. Geophys. Res.*, *85*, 4545-4550, 1980.

Nedoluha, G. E., R. M. Bevilacqua, R. M. Gomez, B. C. Hicks, J. M. Russell III, and B. J. Connor, Ground-based microwave observations of middle atmospheric water vapor in the 1990's, in *Atmospheric Science across the Stratopause*, Geophysical Monograph 123, AGU, Washington, DC, pp. 257-270, 2000.

Nedoluha, G. E., R. M. Bevilacqua, R. M. Gomez, B. C. Hicks, and J. M. Russell III, Measurements of middle atmosphere water vapor from low latitudes in the Northern Hemisphere, 1995-1998, *J. Geophys. Res.*, *104*, 19,257-19,266, 1999.

Olivero, J. J. and G. E. Thomas, Climatology of polar mesospheric clouds, *J. Atmos. Sci.*, *43*, 1263-1274, 1986.

Oltmans, S. J., H. Vomel, D. J. Hofmann, K. H. Rosenlof, and D. Kley, The increase in stratospheric water vapor from balloonborne frostpoint hygrometer measurements at Washington, D.C. and Boulder, Colorado, *Geophys. Res. Lett.*, *27*, 3453-3456, 2000.

Portmann, R. W., G. E. Thomas, S. Solomon, and R. R. Garcia, The importance of dynamical feedbacks on doubled CO_2-induced changes in the thermal structure of the mesosphere, *Geophys. Res. Lett*., *22*, 1733-1736,1995.

Price, J. C., Timing of NOAA afternoon passes, *Int. J. Remote Sens.*, *12*, 193-198, 1991.

Randel, W. J., F. Wu, J. M. Russell III, J. M. Zawodny and J. Nash, Interannual changes in stratospheric constituents and global circulation derived from satellite data, in *Atmospheric Science across the Stratopause*, Geophysical Monograph 123, AGU, Washington, DC, pp. 271-285, 2000.

Rapp, M., et al., Small scale temperature variations in the vicinity of NLC: Experimental and model results, *J. Geophys. Res.*, in press, 2002.

Reid, S. J., A. F. Tuck, and G. Kiladis, On the changing abundance of ozone minima at northern midlatitudes, *J. Geophys. Res.*, 12,169-12,180, 2000.

Remsburg, E. E., P. P. Bhatt, and L. E. Deaver, Seasonal and long-term variations in middle atmosphere temperature from HALOE on UARS, *J. Geophys. Res.*, in press, 2002.

Romejko, V. A., P. A. Dalin, and N. N. Pertsev, 40 years of noctilucent cloud observations near Moscow: database and simple statistics, *to be published in J. Geophys. Res.*, 2002.

Rosenlof, K. H., et al., Stratospheric water vapor increases over the past half-century, *Geophys. Res. Lett.*, *28*, 1195-1198, 2001.

Schlesinger, B. M., and R. P. Cebula, Solar variation 1979-1987 estimated from an empirical model for changes with time in the sensitivity of the Solar Backscatter Ultraviolet instrument, *J. Geophys. Res.*, *97*, 10,119-10,134, 1992.

Shettle, E. P., G. E. Thomas, J. J. Olivero, W. F. J. Evans, D. J. Debrestian, and L. Chardon, Three satellite comparison of polar mesospheric clouds: Evidence for long-term change, *J. Geophys. Res.*, *107*(D12), 10.1029/2001JD000668, 2002a.

Shettle, E. P., S. P. Burton, J. J. Olivero, G. E. Thomas, and L. W. Thomason, SAGE II measurements of polar mesospheric clouds, *to be published in Memoirs Brit. Astron. Assoc.*, *45*, Mesospheric Clouds 2002 (ed. By M. Gadsden and N. D. James), 2002b.

Simmons, D. A. R., and D. H. McIntosh, An analysis of noctilucent clouds over western Europe during the period 1966 to 1982, *Meteorol. Mag.*, *112*, 289-298, 1983.

Stevens, M. H., R. R. Conway, C. R. Englert, M. E. Summers, K. U. Grossman, and O. A. Gusev, PMCs and the water frost point in the Arctic summer mesosphere, *Geophys. Res. Lett.*, *28*, 4449-4452, 2001.

Stolarski, R. S., G. J. Labow, and R. D. McPeters, Springtime Antarctic total ozone measurements in the early 1970s from the BUV instrument on Nimbus 4, *Geophys. Res. Lett.*, *24*, 591-594, 1997.

Taubenheim, J., G. Entzian, and K. Berendorf, Long-term decrease of radiowave reflection heights, *Adv. Space Res.*, *20*, 2059-2063, 1997.

Taylor, M. J., M. Gadsden, R. P. Lowe, M. S. Zalcik, and J. Brausch, Mesospheric cloud observations at unusually low latitudes, *J. Atmos. Solar-Terr. Phys.*, *64*, 991-999, 2002.

Thomas, G. E., Water vapor trends in the mesosphere, paper presented at the Second Workshop "Long-term changes and trends in the atmosphere", Prague, Czech Republic, 2-6 July 2001.

Thomas, G. E., Is the polar mesosphere the miner's canary of global change?, *Adv. Space Res.*, *18*(3), 149-158, 1996.

Thomas, G. E., Climatology of polar mesospheric clouds: Interannual variability and implications for long-term trends, in *The Upper Mesosphere and Lower Thermosphere: A Review of Experiment and Theory*, vol. 87, edited by R. M. Johnson and T. L. Killeen, pp. 185-200, AGU, Washington, DC, 1995.

Thomas, G. E., Solar Mesosphere Explorer measurements of polar mesospheric clouds (noctilucent clouds), *J. Atmos. Terr. Phys.*, *46*, 819-824, 1984.

Thomas, G. E., and C. P. McKay, On the mean particle size and water content of polar mesospheric clouds, *Planet. Space Sci.*, *33*, 1209-1224, 1985.

Thomas, G. E. and J. J. Olivero, Noctilucent clouds as possible indicators of global change in the mesosphere, *Adv. Space Res., 28*, 937-946, 2001.

Thomas, G. E., and J. J. Olivero, Climatology of polar mesospheric clouds, 2. Further analysis of Solar Mesospheric Explorer data, *J. Geophys. Res., 94*, 14,673-14,702, 1989.

Thomas, G. E., R. D. McPeters, and E. J. Jensen, Satellite observations of polar mesospheric clouds by the Solar Backscattered Ultraviolet radiometer: Evidence of a solar cycle dependence, *J. Geophys. Res., 96*, 927-939, 1991.

Thomas, G. E., J. J. Olivero, E. J. Jensen, W. Schroder, and O. B. Toon, Relation between increasing methane and the presence of ice clouds at the mesopause, *Nature, 338*, 490-492, 1989.

Twomey, S., On the deduction of the vertical distribution of ozone by ultraviolet spectral measurements from a satellite, *J. Geophys. Res., 66*, 2153-2162, 1961.

von Cossart, G., J. Fiedler, and U. von Zahn, Size distributions of NLC particles as determined from 3-color observations of NLC by ground-based lidar, *Geophys. Res. Lett., 26*, 1513-1516, 1999.

von Zahn, U., Temperature and altitude of the polar mesopause in summer, *Adv. Space Res., 10*, (12)223-(12)231, 1990.

Wickwar, V. B., M. J. Taylor, J. P. Herron, and B. A. Martineau, Visual and lidar observations of noctilucent clouds above Logan, Utah, at 41.7°N, *J. Geophys. Res., 107*(D7), 10.1029/2001JD001180, 2002.

Woods, T. N., and G. J. Rottman, Solar Lyman α irradiance measurements during two solar cycles, *J. Geophys. Res., 102*, 8769-8779, 1997.

Woods, T. N., W. K. Tobiska, G. J. Rottman, and J. R. Worden, Improved solar Lyman α irradiance modeling from 1947 through 1999 based on UARS observations, *J. Geophys. Res., 105*, 27,195-27,215, 2000.